Universidad Carlos III de Madrid
Escuela Politécnica Superior

RENDEZVOUS IN NON KEPLERIAN ORBITS

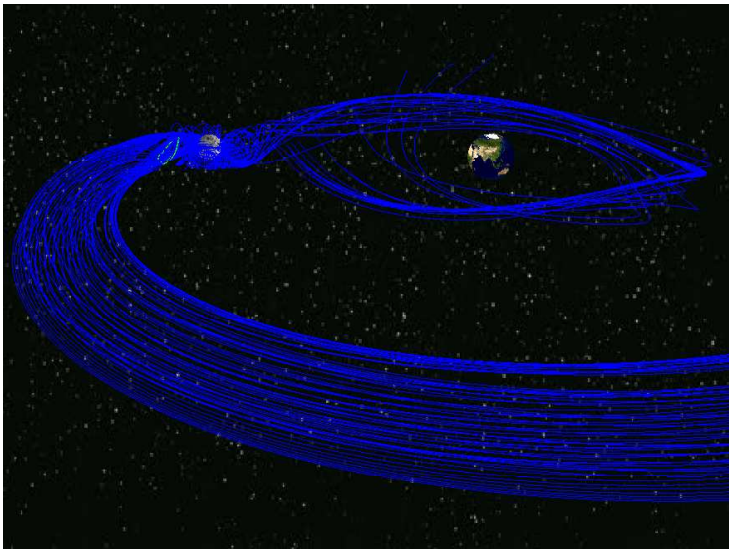

A master thesis submitted in fulfillment of the requirements for the Master in Aeronautic Engineering

Academic Year 2017/2018

Author: Rubén Vega Astorga
Director: Manuel Sanjurjo

Abstract

The main goal of this thesis is designing a space trajectory which allows to make rendezvous at an arbitrary non-keplerian trajectory. In particular, this thesis has focus in the non-keplerian trajectories that are originated in the Earth-Moon system. A thorough study of this system dynamical characteristics has been performed at first. Then, the dynamical properties of some particular non-keplerian trajectories (i.e L_1 halo orbits, NRO and L_2 halo orbits) have been analyzed so as to analyze their feasibility for making a rendezvous mission. Finally, an exhaustive analysis of how performing a rendezvous mission in a non-keplerian orbit has been presented in detail. This analysis has been particularized for an L_2 Halo orbit, providing an example of the challenges that must be faced during the design analysis of this kind of missions.

Acknowledgements

First of all I would like to thank my family, who have always support me in all the projects I have undertaken.

Secondly, I would like to express my gratitude to Manuel Sanjurjo for aiming me to undertake a project in such fascinating field and giving me the best academical support every time I needed with the highest dedication.

Finally, I would like to thank to all those friends that have encouraged me during the project.

Contents

List of Acronyms

$CRTBP$: Circular Restricted Three Body Problem

DRO: Distant Retrograde Orbit

EP: Electric Propulsion

ESA: European Space Agency

$IPOPT$: Interior Point Optimizer

LLO: Low Lunar Orbit

$NASA$: National Aeronautics and Space Administration

NRO: Near Rectilinear Orbit

PCO: Prograde Circular Orbit

STM: State Transition Matrix

List of Figures

List of Tables

Chapter 1

Introduction

Space exploration is a field in continuous development. New missions are aspired every year aiming to overpass human current technological limitations. This rising complexity yields the necessity to investigate unusual orbits and propulsive improvements which would be able to bear the upcoming challenges. In particular, pre-eminent space agencies such as NASA or ESA are leading last progress in trajectory design in preparation for deep space exploration. A clear objective has already been defined for the near future: human settlement on Mars. With this aim, recent research of the Earth-Moon system has been undertaken to look for emplacements which could work as space base for supporting those missions. It has been noticed that cis-lunar and beyond-lunar space environment might be a great slightly explored opportunity. Hence, the capability of rendezvous in those emplacement seems to be crucial to meet the resolved objectives. To focus in the analysis of the design challenges of this field of study has motivated this thesis.

In this chapter, an overview of the whole project is presented. The current state of the art is introduced to understand the motivation of this thesis and the goals that have originated it. Then, the methodology followed in order to meet the thesis objectives is presented, including the designed time planning that have supported the successfully achievement of those. Finally, a general overview of this thesis structure is going to be explained, in order to help the reader with the understanding of the project.

1.1 History

Interest in space exists since human history commences. Ancient humans curiosity leads to wonder about the celestial structures and spheres which could be observed from Earth. Then, the appearance of the first astronomers studying the movement of those celestial bodies promptly become a reality. For many centuries, space was a field of exploration developed by many important scientists, such as Ptlolomy, which develops one of the first models describing those celestial body movements; Copernicus, which improved those studies by developing an Heliocentric model describing those motions as oppose to the Geocentric ptolemaic model; Kepler, which primary realized about the eccentricity of the solar orbits; and Newton, which introduce the dynamical laws which govern the motion of celestial bodies. Nonetheless, all these studies were theoretical, based on the observations and measures they can take from Earth. Space exploration was not feasible until the development of rocket technology.

Primitive rockets were invented in ancient China around the 1200 AC as weapons, from which they quickly widespread in Europe. It was not until the XIX centuries when this technology witness a significant development, but again as weapons. During the end of that century and the beginnings of the XX century it was developed all the theoretical and practical basis which allowed the later success of this technology in providing space access capability. This development was not possible unless the work of some renowned technologist such as K.E. Tsiolkovsky, who set the theoretical basis of rockets; R.H. Goddard, that was able to test the first liquid propellant rocket in 1926; and H. Oberth, who introduced visionary ideas such as staging or rocket walls film cooling.

Recently, space propulsion technology continues being developed. In particular, the electric propulsion thrusters invention has spread in a significant way the human space exploration capabilities. EP thrusters are characterized for providing large specific impulse values (I_{sp}), which has allowed to broaden the distance that spacecraft can travel through space. Hence, new challenging and demanding missions are aimed nowadays, procuring gain deeper knowledge about the space surrounding and overpassing human limits.

1.2 State of the Art

Spaces agencies such as NASA and ESA are targeting the design of new missions to reach deep space destinations. Among others, the human settlement in Mars is a known goal. With such purpose, it is planning to use staging orbits with the capability of providing support for conducting such in-space missions while it is also afforded support for lunar surface activities and intermediate step to Mars transfer orbits. According to recent studies [2], cislunar and beyond space environment orbits seems to fulfil the desired requirements for the upcoming space missions.

1.2.1 The Cis-Lunar Space Environment

Cis-lunar space environment offers a huge variety of distinct orbits that can be targeted as stage orbits for in-space missions. Each of them particularly provides some benefits which could positively impact in the cost of deep space missions. In fact, due to the closely influence of both the Earth and the Moon celestial bodies, the orbits do not fulfil the classical Keplerian behaviour, which yields a widen set of available trajectories. The most relevant orbits for such mission have been found to be the following ones according to [2].

- *Low Lunar Orbits (LLO) and Elliptical Lunar Orbits (ELO).* They are the classical Keplerian orbits which can be found in the moon neighbourhood. The well knowledge for these kind of orbits seems to be one of the greatest advantages for such orbits. Also, its proximity to lunar surface makes this orbits ideals for supporting surface operations.

- *Prograde Circular Orbits.* These are moon orbits which are characterized by rotating in the prograde direction. They have been discovered to be very stable, implying that few corrections manoeuvres are necessary for keeping an spacecraft on it.

- *Earth-Moon Libration Point Orbits.* They are some orbits that get originated at the vicinity of the Lagrange Libration points of the Earth-Moon system. They are also known as Halo orbits, due to the fact that these kind of orbits look like an “halo” of the Moon when viewed from Earth. Because of its vicinity to the Libration points, they are characterized by keeping its position with respect to Earth, which facilitated tracking and controlling objects at those orbits from the Earth. From all these orbits, it has been noticed according to various

sources that Halo orbits around the L_2 point seem to be favourable for future human missions [3].

- *Near Rectilinear Orbits (NRO).* The orbits were discovered such a bridge between L_1 and L_2 Halo orbits. Although they seem to rotate through the Moon poles, they are actually rotating around the Earth at the same rate than the Moon, so that similar features to the Halo orbits are found.

Orbit	**Earth**	**Moon**	**Crewed Spacecraft**		
Type	**Access**	**Access**	Station Keeping	Communication	Thermal
LLO	Infeasible	Feasible	Low-medium	50% Oculted	Radiators Insufficient
PCO	Marginally Feasible	Marginally feasible	Optimal	Unknown	Unknown
ELO	Marginally Feasible	Marginally infeasible	Demanding	Frequent Occultation	Unknown
L2-Halo	Feasible	Marginally infeasible	Very low	No Occultation	Radiators Insufficient
NRO	Feasible	Marginally feasible	Very low	No Occultation	Radiators Insufficient

Table 1.1: Staging Orbit Summary Comparison. [2]

1.2.2 Cis-Lunar orbit types: benefits ans drawbacks

The more relevant orbits found in the Cis-Lunar environment have been analyzed assessing its performance in respect to different criteria. A brief summary is provided hereafter.

Three main aspects has been considered in this analysis: the Earth accessibility, the Lunar accessibility and the impacts that a crewed spacecraft would face in that orbit, involving the required station keeping, communication to Earth capability and the thermal environment to be

supported. Results are sorted in Table 1.1. For a thorough explanation of these comparison, please refer to [2].

From this analysis, it has been concluded that regarding the cis-lunar space and beyond environment, L_2 halo orbits NRO appear to be the most favourable option for meeting the conditions previously described. In addition, since crewed travel into deep space are targets for the near future, parking orbits from which establishing a base of operations will be needed, aspects which are greatly covered by these orbits. Indeed, a great communication capability due to the eclipse absence in that orbits and the good Earth accessibility are extremely important to safely carry out missions with on-board crew.

1.3 Goals

From the state of the art regarding the upcoming space exploration challenges, it has deduced that both L_2 halo orbits and NRO are potential orbits from where operate the in-space missions. Thus, rendezvous in those orbits is a necessity whose importance will exponentially increase in the next years. Study the rendezvous mission in those kind of orbits is the primary objective of this thesis.

In addition, some global aspects are expected to be gain during this project. For clarity purposes, they are summarized hereafter.

- The implication of two massive bodies in the motion of the spacecraft which is aimed to reach L_2 Halo orbit and NRO destination.
- The derivation of the Circular Restricted Three Body Problem (CRTBP) equations of motion.
- Describing spacecraft movement in respect the target rendezvous body.
- The comprehension of the most relevant orbits that can be originated in the Earth-Moon system.
- The dynamical characteristics of those kind of orbits, involving the manifold concept.
- The implementation of a reliable numerical program able to solve the control optimization problem which the non-keplerian rendezvous mission implies.

- A throughout understanding of the main characteristics driven the rendezvous problem.

1.4 Methodology & Time planning

As any challenging project, a methodology of work must be defined in order to provide a series of tools which help to achieve the defined objectives. A structured plan of action has been developed to carry out during the project. Tasks definition has been stated and an accurate time planning has been done.

A Gantt diagram is a project management tool which allows to establish a time planning of the project. The one regarding the project on purpose is presented in Figure 1.1.

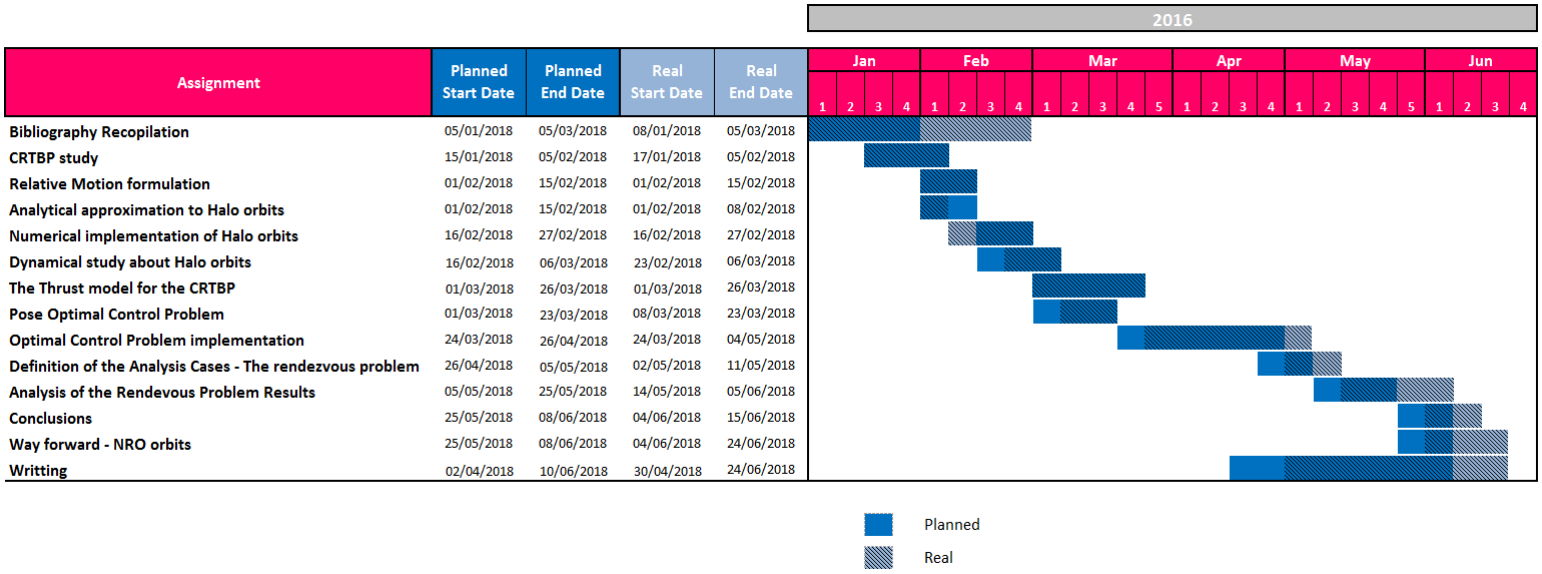

Assignment	Planned Start Date	Planned End Date	Real Start Date	Real End Date
Bibliography Recopilation	05/01/2018	05/03/2018	08/01/2018	05/03/2018
CRTBP study	15/01/2018	05/02/2018	17/01/2018	05/02/2018
Relative Motion formulation	01/02/2018	15/02/2018	01/02/2018	15/02/2018
Analytical approximation to Halo orbits	01/02/2018	15/02/2018	01/02/2018	08/02/2018
Numerical implementation of Halo orbits	16/02/2018	27/02/2018	16/02/2018	27/02/2018
Dynamical study about Halo orbits	16/02/2018	06/03/2018	23/02/2018	06/03/2018
The Thrust model for the CRTBP	01/03/2018	26/03/2018	01/03/2018	26/03/2018
Pose Optimal Control Problem	01/03/2018	23/03/2018	08/03/2018	23/03/2018
Optimal Control Problem implementation	24/03/2018	26/04/2018	24/03/2018	04/05/2018
Definition of the Analysis Cases - The rendezvous problem	26/04/2018	05/05/2018	02/05/2018	11/05/2018
Analysis of the Rendevous Problem Results	05/05/2018	25/05/2018	14/05/2018	05/06/2018
Conclusions	25/05/2018	08/06/2018	04/06/2018	15/06/2018
Way forward - NRO orbits	25/05/2018	08/06/2018	04/06/2018	24/06/2018
Writting	02/04/2018	10/06/2018	30/04/2018	24/06/2018

Figure 1.1: Gantt diagram.

1.5 Thesis structure

This thesis has been divided in several chapters. Its structure is presented below:

1. In the second chapter, the Circular Restricted Three Body problem is studied in detail. The governing equations of motion are clearly stated and an overview about the in a rendezvous mission possible reference frames is performed.

2. The third chapter focuses in the analysis of the destination orbits at which rendezvous is targeted in the near future: collinear Halo orbits and NRO. An analytical and a numerical method for finding such orbits are presented together with a throughout study of their dynamical characteristics.

3. Fourth chapter presents the project results. At first, the rendezvous optimal control problem is introduced in order to familiarize the reader with the constraints faced when solving the problem. Rendezvous in L_2 halo orbit has been the focus of the study, since these orbits group the main features than non-keplerian orbits in the Earth-Moon system share. Then, an exhaustively analysis of the obtained results are performed to ensure a correct understanding and implications of the non-keplerian rendezvous problem.

4. Finally, some conclusions and future lines of research are drawn in the fifth chapter.

Chapter 2

Circular Restricted Three Body Problem

In this chapter, a detailed analysis of the Circular Restricted Three Body Problem (CRTBP) is carried out. The aim of this analysis is fully describing the concepts and the model which are needed for spacecraft trajectory design in the vicinity of the Earth-Moon system, a study case where the spacecraft is moving near two massive bodies.

This chapter is roughly divided in two parts. At first, the equations of motion describing the problem are presented, once the model assumptions are clearly stated. Then, the resulting dynamical system is analyzed in order to understand the particularities arisen from the fact that a new massive body is affecting the solution, as opposed to classical Keplerian orbits. Lastly, a brief insight about expressing the equations of motion respect to a target moving reference frame is performed.

2.1 Theoretical Background and Assumptions

In contrast to the Two Body Problem, where differential equations with an analytical solution can be easily derived, the presence of a new massive body to the problem makes the problem intractable that way. Two main challenges are encountered when facing this new problem:

- The motion is no longer planar.
- The Three Body Problem actually exhibits deterministic chaos, so that a tiny change in the problem initial conditions could lead to completely different trajectory evolution in time.

So as to solve those challenges, a set of assumptions have been settled to start facing the problem.

2.1.1 CRTBP assumptions

Quite accurate approximation is attained when treating the Earth-Moon Three Body Problem as a Circular Restricted Three Body Problem (CRTBP), since it greatly adjusts to all the assumptions involved in this theory development. These assumptions are depicted next.

- From the three masses involved in the problem, only two of those are considered to be massive body. The third one, which corresponds to the spacecraft mass, is considered to be negligible in comparison of the other two.
- The two massive bodies move in circular orbits about their common center of mass. This motion is supposed to be unaffected by the third body mass in consequence of the previous assumption.
- There are not any external forces disturbing the third body motion.

The third body motion analysis in the two massive body masses system under the aforementioned conditions is what takes the name of circular, restricted, three body problem (CRTBP).

2.1.2 Problem adimensionalization

In order to procure a general solution of the CRTBP, the problem is going to be made non-dimensional. These allow us to gain a general understanding of the physics behind this kind of problems whatever the body masses systems analyzed.

For the sake of clarity, from now on the most massive body is going to be called the primary mass (m_1), and the other massive body will be named the secondary mass (m_2). Then, the characteristic units for the CRTBP can be described.

- *Characteristic mass* M_c: It is taken to be the sum of the two massive bodies: $M_c = m_1 + m_2$
- *Characteristic length* L: It has been defined as the constant distance separation between the primary and the secondary mass.
- *Characteristic time* T_c: It is the time at which the orbital period of the two massive masses is equal to 2π.

From these selected characteristic values, it results that the universal constant of gravitation (G) for the CRTBP then becomes equal to the unity. Also, the common mean motion of the massive bodies, n, becomes equal to one. Then, the derivation of the relationships between dimensional and non-dimensional magnitudes are straightforward. Hereafter, it is presented the main relations which are going to be needed along this thesis.

$$d' = L_c \cdot d \qquad v' = V_c \cdot v = \frac{L_c}{T_c} \cdot v$$

$$t' = T_c \cdot t \qquad a' = A_c \cdot a = \frac{L_c}{T_c^2} \cdot a$$

The primed letters correspond to the dimensional values, and the unprimed letters to the non-dimensional ones. d refers to distance, v to velocity, a to accelerations and t to times.

An additional parameter must be then introduce in order to be able to particularize the problem for every given CRTBP. With this purpose, it is used the **mass parameter**, which highly affects the phase space of the system. It is defined as:

$$\mu = \frac{m_2}{m_1 + m_2} \tag{2.1}$$

In particular, for the thesis three body system of interest, the Earth-Moon one, it has been calculated the conversion factors between dimensional and non-dimensional parameters, and its mass parameter.

$\mu\,(-)$	$T_c\,(s)$	$L_c\,(km)$
$1.215058561 \cdot 10^{-2}$	$3.75699807501 \cdot 10^{5}$	$3.84388174 \cdot 10^{5}$

Table 2.1: Mass parameter and conversion factors for the Earth-Moon system.

2.2 Equations of Motion Development

There are several methods that can be used for deriving the equations of motion for a given problem. Choosing one, usually results from a trade-off comparison between the advantages and disadvantages of each of them. Here, the classical Newtonian approach will be presented, together with the Lagrangian approach, which particularly offers a simple method for finding the final equations of motion in this study case.

2.2.1 Reference frames

For describing mathematically the trajectory of a given particle, firstly it is necessary to define appropriate reference frames and position vectors. The choice of a smart reference frame is crucial for either reaching the final equations in a simpler way or for helping the analysis of the final results, since there are frames where it can be easily understood how the motion of a particle is taking place. For the Earth-Moon CRTBP, two main reference frames make sense to be defined.

Inertial Reference Frame

The inertial reference frame for this system is defined in the following way. Its origin is located at the center of mass of the massive bodies $m_1 - m_2$ system. Then, a orthogonal reference frame is constructed with two axis in the orbital plane of motion of the two bodies, and the third one in the perpendicular direction to that plane, as it can be observed in Fig.[2.2.1].

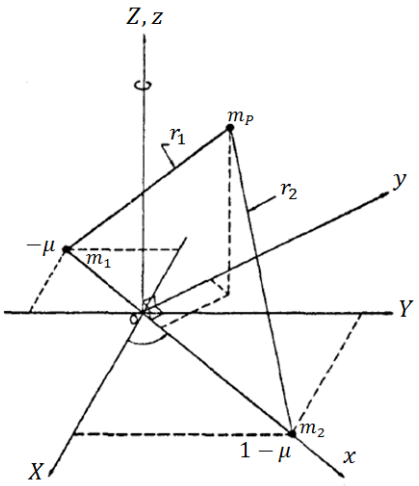

Figure 2.1: Geometry of the three-body problem. [1]

Rotating Reference Frame

Since what it is intended to study is the spacecraft motion relative to the two massive bodies, selecting a rotating frame which moves with the main bodies is useful for such purpose. Again, the origin of this reference frame is located at the system center of mass. Then, x-coordinate is directed along the secondary mass position and then, the other two axes are set orthogonal, being the y-coordinate contained in the two massive bodies plane of motion. It can be observed in Fig.[2.2.1] that the massive body position respect to the rotating reference frame is only dependent on the mass parameter. The point P refers to the spacecraft mass.

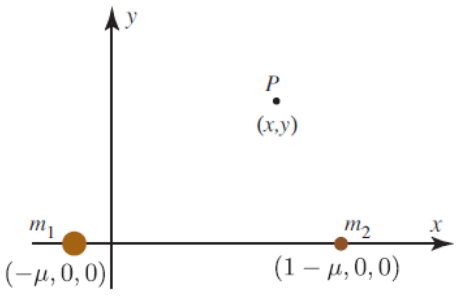

Figure 2.2: Inertial ref. frame

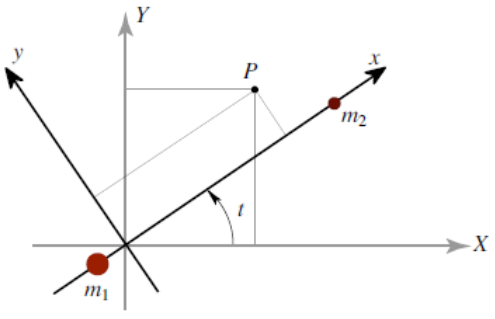

Figure 2.3: Ref. frames relation

The coordinate transformation between both references frames must be

defined then. Both frames share same z-axis, which is indeed the rotation axis for the coordinates transformation.

$$\begin{bmatrix} X \\ Y \\ Z \end{bmatrix} = A_t \cdot \begin{bmatrix} x \\ y \\ z \end{bmatrix} = \begin{bmatrix} cos(t) & -sin(t) & 0 \\ sin(t) & cos(t) & 0 \\ 0 & 0 & 1 \end{bmatrix} \cdot \begin{bmatrix} x \\ y \\ z \end{bmatrix} \tag{2.2}$$

X, Y and Z capital letters denote that the spacecraft position is being given in the Inertial reference frame coordinates whilst the lower case letters means that the position is referred to the rotating one. A_t is the transformation matrix.

$$\begin{bmatrix} \dot{X} \\ \dot{Y} \\ \dot{Z} \end{bmatrix} = \dot{A}_t \cdot \begin{bmatrix} x \\ y \\ z \end{bmatrix} + A_t \cdot \begin{bmatrix} \dot{x} \\ \dot{y} \\ \dot{z} \end{bmatrix} = A_t \cdot \begin{bmatrix} \dot{x} - y \\ \dot{y} + x \\ \dot{z} \end{bmatrix} \tag{2.3}$$

where

$$\dot{A}_t = \begin{bmatrix} -sin(t) & cos(t) & 0 \\ cos(t) & -sin(t) & 0 \\ 0 & 0 & 1 \end{bmatrix} \tag{2.4}$$

Although for the CRTBP case analyzed it is more convenient to use the rotating reference frame, the inertial one will always be useful for combining the CRTBP results in systems where larger amount of bodies were involved, as for instance, the complete solar system.

2.2.2 Gravitational Potential

The adimensional gravitational potential which a particle P would experience due to the presence of the massive masses m_1 and m_2 is given by the following expression.

$$U = -\frac{\mu_1}{r_1} - \frac{\mu_2}{r_2} - \frac{1}{2}\mu_1\mu_2 \tag{2.5}$$

Note that r_1 and r_2 are the distances comprehended between m_1 and m_2 respectively. Depending on the chosen reference frame, the gravitational potential will be dependent or not on time. Recall that for the inertial reference frame, these variables would take this form.

$$r_1^2 = (X + \mu cos(t))^2 + (Y + \mu sin(t))^2 + Z^2 \tag{2.6}$$
$$r_2^2 = (X + (\mu - 1)cos(t))^2 + (Y + (\mu - 1)sin(t))^2 + Z^2 \tag{2.7}$$

2.2.3 Newtonian approach

Given the gravitational potential U previously defined, the Newtonian equations of motion take the following form in the Inertial reference frame. The gravitational potential subscripts indicates the variable from which the partial derivative of U must be calculated. Note that the subscripts letters refers to the inertial reference frame, since this Newton's expression only holds for this kind of systems.

$$\ddot{X} = -U_X; \qquad \ddot{Y} = -U_Y; \qquad \ddot{Z} = -U_Z; \tag{2.8}$$

This system is time dependent when expressed respect to the inertial reference from. This time dependence can be eliminated when transforming the X, Y, Z, t variables from the resulting equations into x, y, z by direct computation. This can be simply done by using the variable transformation equations given (eq.2.2 & eq.2.3).

2.2.4 Lagrangian approach

The Newton's method explained before involves taking a large amount of operations. On the contrary, Lagrangian approach offers a simpler method for deriving those equations for this particular system. Being aware of the distinct advantages and disadvantages that different approaches offer depending on the physical system analyzed allow to develop the equations of motion in a smart way. In fact, the theory of moving systems says that by simply writing the Euler-Lagrange equations in the moving reference frame, the right equations of motions are got. Then, for this reason, Lagrangian approach is going to be thoroughly commented next.

Let's consider the Euler-Lagrangian equations with generalized coordinates q_i describing the mechanical system.

$$\frac{d}{dt}\frac{\partial L}{\partial \dot{q}^i} - \frac{\partial L}{\partial q^i} = 0 \tag{2.9}$$

Taking the Lagrangian the form of the kinetic energy minus the potential energy, as it is usually done in this approach according to [4], it is obtained in the inertial frame the following expression.

$$L(X, Y, Z, \dot{X}, \dot{Y}, \dot{Z}, t) = \frac{1}{2}\left(\dot{X}^2 + \dot{Y}^2 + \dot{Z}^2\right) - U(X, Y, Z, t) \tag{2.10}$$

Again, the resulting equation is time-dependent. Nevertheless, by expressing it respect to the rotating reference frame, the system then becomes time-independent, which greatly simplify the analysis. Using the transformation relationship from eq.2.3, the kinetic term can be expressed as:

$$\frac{1}{2}\left(\dot{X}^2 + \dot{Y}^2 + \dot{Z}^2\right) = \frac{1}{2}\left[(\dot{x} - y)^2 + (\dot{y} + x)^2 + \dot{z}^2\right] \tag{2.11}$$

Regarding the potential energy term, the transformation just consists on expressing r_1 and r_2 variables in the rotating reference frame (see eq.2.26-27). Finally, the Lagrangian of the system becomes:

$$L(x, y, z, \dot{x}, \dot{y}, \dot{z}) = \frac{1}{2}\left[(\dot{x} - y)^2 + (\dot{y} + x)^2 + \dot{z}^2\right] - U(x, y, z) \tag{2.12}$$

Introducing the Lagrangian into eq.2.9, the following equations are obtained.

$$\frac{d}{dt}(\dot{x} - y) = \dot{y} + x - U_x \tag{2.13}$$

$$\frac{d}{dt}(\dot{y} + x) = (\dot{x} - y) - U_y \tag{2.14}$$

$$\frac{d}{dt}z = -U_z \tag{2.15}$$

Please, note that the subscripts express the variable from which the partial derivative of the gravitational potential is taken. As oppose to the previous Newtonian approach, these mentioned partial derivatives are taken respect to the rotating reference frame. Simplifying this set of equations (eq.2.13-15), the equations of motion for the CRTBP are obtained.

$$\ddot{x} - 2\dot{y} = x - U_x = -\bar{U}_x \tag{2.16}$$

$$\ddot{y} + 2\dot{x} = y - U_y = -\bar{U}_y \tag{2.17}$$

$$\ddot{z} = -U_z = -\bar{U}_z \tag{2.18}$$

Grouping all the acceleration terms depending on the spacecraft position ($[x, y, z]^T$), an augmented or effective gravitational potential $\bar{U}$ can be defined.

$$\bar{U} = -\frac{1}{2}\left(x^2 + y^2\right) + U(x, y, z) \tag{2.19}$$

2.3 CRTBP Equations of Motion

The following set of ordinal differential equations defines the spacecraft movement at any three body system (given by the mass parameter μ). They are presented written in first-order form.

$$\dot{x} = v_x \tag{2.20}$$
$$\dot{y} = v_y \tag{2.21}$$
$$\dot{z} = v_z \tag{2.22}$$
$$\dot{v_x} = 2v_y + x - \frac{(1-\mu)(x+\mu)}{r_1^3} - \frac{\mu(x-1+\mu)}{r_2^3} \tag{2.23}$$
$$\dot{v_y} = -2v_x + y - \frac{(1-\mu)y}{r_1^3} - \frac{\mu y}{r_2^3} \tag{2.24}$$
$$\dot{v_z} = -\frac{(1-\mu)z}{r_1^3} - \frac{\mu z}{r_2^3} \tag{2.25}$$

where

$$r_1 = \sqrt{(x+\mu)^2 + y^2 + z^2} \tag{2.26}$$
$$r_2 = \sqrt{(x-1+\mu)^2 + y^2 + z^2} \tag{2.27}$$

2.4 The Jacobi Integral

Deriving an analytical solution for the set of ordinary differential equations describing the CRTBP is not possible. Nonetheless, some methods have been developed for analytically deriving equations which at least provide a qualitative knowledge about the problem. One of those is the Jacobi integral.

The Jacobi integral [5], or also called the Jacobi constant, is the energy equation of the system expressed in the rotating frame. It can be assessed

its existence since all the forces that make work can be written in a potential form ($\bar{U}$). It can be derived by following this procedure.

$$\begin{aligned}\dot{x}\ddot{x} + \dot{y}\ddot{y} + \dot{z}\ddot{z} &= \dot{x}\left(2v_y - \frac{\partial \bar{U}}{\partial x}\right) + \dot{y}\left(-2v_x - \frac{\partial \bar{U}}{\partial y}\right) + \dot{z}\left(-\frac{\partial \bar{U}}{\partial z}\right) \\ &= \frac{\partial \bar{U}}{\partial x}\dot{x} + \frac{\partial \bar{U}}{\partial y}\dot{y} + \frac{\partial \bar{U}}{\partial z}\dot{z} = \frac{d}{dt}\left(-\bar{U}\right)\end{aligned} \tag{2.28}$$

On the other hand, if the relative kinetic energy is derived by time, it can be related with the above equation.

$$\frac{d}{dt}\left(\dot{x}^2 + \dot{y}^2 + \dot{z}^2\right) = 2\dot{x}\ddot{x} + \dot{y}\ddot{y} + \dot{z}\ddot{z} = \frac{d}{dt}\left(-2\bar{U}\right) \tag{2.29}$$

Integrating eq.2.29, the Jacobi constant is obtained.

$$C(x, y, z, \dot{x}, \dot{y}, \dot{z}) = -\left(\dot{x}^2 + \dot{y}^2 + \dot{z}^2\right) - 2\bar{U} \tag{2.30}$$

Note that the Jacobi constant sign is opposite to the one that would have the total energy (E) of the system. Therefore, considering an increase of the system total energy is equivalent to reduce the Jacobi constant of the system. Please, recall that the total energy of the system would be:

$$\frac{v^2}{2} + \bar{U} = E \tag{2.31}$$

where v is the relative total velocity of a particle in the CRTBP, being $v^2 = (\dot{x}^2 + \dot{y}^2 + \dot{z}^2)$.

2.4.1 Hill Regions

By using the Jacobi integral, regions of possible motion can be analyzed of existence for the spacecraft given a value of the Jacobi constant (or total energy). This region would be all the spacecraft positions with relative kinetic energy greater than zero ($v^2 > 0$). [6][7]

From this analysis, it can be understood some basic concepts about a mass moving in the CRTBP. For instance, for large Jacobi constant values, the spacecraft can only be very close to the massive bodies or very far from them. Then, as long as the Jacobi constant is reduced (which involves that the total energy of the system is increased), the region of existence for the spacecraft starts to grow. During this process, it can be calculated the minimum value

of energy (E) or Jacobi constant value which let the spacecraft travel from one massive mass to the another one.

The Jacobi integral also lets introduce the idea of equilibrium surfaces in the CRTBP. In fact, for a given Hill region, there is a surface boundary where the relative velocity of the spacecraft goes to zero, which are known as *Zero Velocity curves* . Actually, these surfaces are the contour surfaces of the potential function. Therefore, the motion of a vehicle at those systems is driven by the gradient of the potential function ($\nabla \bar{U}$). Looking at the case at which this gradient equals zero, it can be stated that the gravitational and centrifugal forces will cancel out, thus the spacecraft will remain and that position in the rotating reference frame. These particular points are known as Lagrange points. They are the equilibrium solution for the CRTBP.

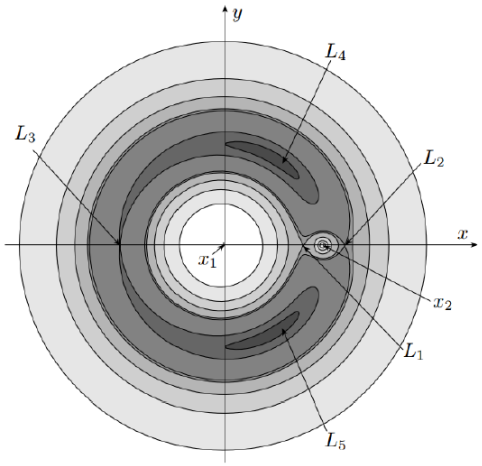

Figure 2.4: Zero velocity Hill Regions.

2.5 The equilibrium points

Exploring the Jacobi integral concept provide an overall comprehension of the spacecraft motion and the existence of equilibrium. For the problem which is intended to be solved, it is necessary to accurately know the position of these points, since Halo orbits are a special kind of orbits that are formed in the Lagrangian points neighbourhood.

The Lagrangian points for the CRTBP are located in the rotational x-y plane as it can be appreciated in Fig.2.5. The symbols appearing in this picture will be used as reference for the calculation which are going to be

presented.

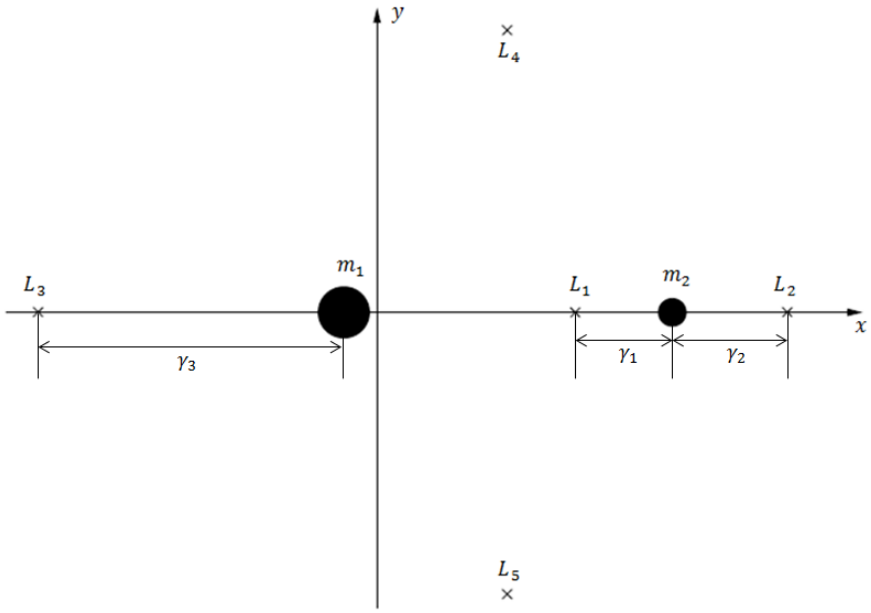

Figure 2.5: The CRTBP Libration points given in the rotating reference frame.

As described when analyzing the Hill regions, there exists five equilibrium points: three collinear on the x-axis, called L_1,L_2 and L_3; and two equilateral named L_4 and L_5. They can be obtained by equating the right-hand side of the CRTBP (eq.2.20-25) to zero [8]. Promptly, it is deduced that the solution will have the form $[x^*, y^*, 0, 0, 0, 0]^T$, meaning that the solution will be contained in the x-y plane and that the velocity (relative to the rotating reference frame) will be null.

2.5.1 The equilateral equilibrium points

At first, the solution which does not lie on the line joining the two massive masses is going to be investigated. For such purpose, the following relation must be noticed, where the distances given by r_i are the ones showed in eq.2.26-27.

$$x^2 + y^2 = (1-\mu)r_1^2 + \mu r_2^2 - \mu(1-\mu) \tag{2.32}$$

Introducing this equation into the augmented or effective gravitational potential (eq.2.19), it yields:

$$\bar{U}(r_1, r_2) = -\frac{1}{2}(1-\mu)r_1^2 - \frac{1}{2}\mu r_2^2 - -\frac{1-\mu}{r_1} - \frac{\mu}{r_2} \tag{2.33}$$

It can be shown by applying the chain rule that both $\bar{U}(x, y)$ and $\bar{U}(r_1, r_2)$ share the same critical points.

$$\bar{U}_x = \bar{U}_{r_1}\frac{\partial r_1}{\partial x} + \bar{U}_{r_2}\frac{\partial r_2}{\partial x} = \bar{U}_{r_1}\frac{x+\mu}{r_1} + \bar{U}_{r_2}\frac{x-(1-\mu)}{r_2} = 0 \tag{2.34}$$

$$\bar{U}_y = \bar{U}_{r_1}\frac{\partial r_1}{\partial y} + \bar{U}_{r_2}\frac{\partial r_2}{\partial y} = \bar{U}_{r_1}\frac{y}{r_1} + \bar{U}_{r_2}\frac{y}{r_2} \tag{2.35}$$

Then, finding the equilateral solutions in the system given by eq.2.20-25 would be equivalent to find these solutions in the upcoming system.

$$0 = -\bar{U}_{r_1} = \mu r_2 - \frac{\mu}{r_2^2} \tag{2.36}$$

$$0 = -\bar{U}_{r_2} = (1-\mu)r_1 - \frac{1-\mu}{r_2^2} \tag{2.37}$$

The solution for this system is unique: $r_1 = r_2 = 1$. This solution implies that the these equilibrium points will form an equilateral triangle with respect to the massive masses. This condition is fulfilled by only two points in the CRTBP, the ones denominated L_4 and L_5. By convention, the former corresponds to the solution lying in the positive y-axis whilst the later lies in the negative one, as it is presented in Fig.2.5.

2.5.2 The collinear equilibrium points

Seeking the collinear equilibrium solutions imply that $y^* = 0$ is a necessary condition. Therefore, the system of equations to solve is reduced to a single expression.

$$\frac{\partial}{\partial x}\bar{U}(x^*, 0, 0) = 0 \tag{2.38}$$

Working on the above equation, it can be obtained a quintic order equation for each collinear equilibrium solution [9]. For the L_1 and L_2 solutions, this polynomial equation is presented hereafter. Note that the

upper sign corresponds to the L_1 solution (γ_1) and the lower sign to the L_2 solution.

$$\gamma^5 \mp (3-\mu)\gamma^4 + (3-2\mu)\gamma^3 - \mu\gamma^2 \pm 2\mu\gamma - \mu = 0 \tag{2.39}$$

As first approximation, expansion series can be used for finding such solution. For instance, for L_1 and L_2 points, this approximation takes the following form.

$$\gamma_1 = r_h \left(1 - \frac{1}{3}r_h - \frac{1}{3}r_h^2 + ...\right)$$
$$\gamma_2 = r_h \left(1 + \frac{1}{3}r_h - \frac{1}{3}r_h^2 + ...\right)$$

Note that r_h refers to the Hill radius, which is given by this equation.

$$r_h = \left(\frac{\mu}{3}\right)^{\frac{1}{3}} \tag{2.40}$$

For the Earth-Moon system, the L_1 and L_2 points location positions have been calculated. This information is needed for retrieving the Halo orbits.

$$\gamma_1 = 0.150934288618019 \qquad \gamma_2 = 0.167832751054508 \tag{2.41}$$

Please, refer to Fig.2.5 so as to understand the physical meaning of these achieved values. Note that they are magnitudes, so that:

$$r_{L_1} = x_{m_2} - \gamma_1 = 1 - \mu - \gamma_1 \qquad r_{L_2} = x_{m_2} + \gamma_2 = 1 - \mu + \gamma_2 \tag{2.42}$$

2.6 Relative Motion

A rendezvous mission implies that two spacecraft are moving under the same mechanical system laws at the same time. For such cases, sometimes is useful to make use of relative motion equations of motion. In this way, it is possible to constantly refer the chasing position to the target one, providing a better perception about the rendezvous mission status. The derivation of the relative equations of motion for the CRTBP is presented hereafter.

At first, the relative position vector $\vec{s}$ must be defined. It joins the target and the chaser vehicles, being originated at the target position.

$$\vec{r}_t + \vec{s} = \vec{r}_c \rightarrow \vec{s} = \vec{r}_c - \vec{r}_t \tag{2.43}$$

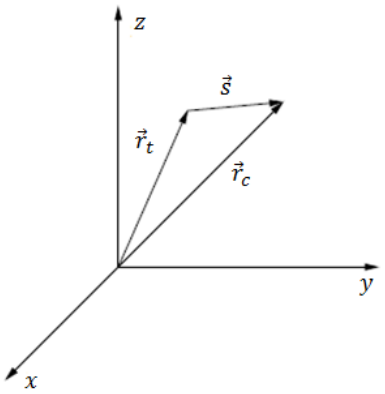

Figure 2.6: Vectors definitions for the Relative Motion problem.

Deriving this equation in time and using the CRTBP equations (eq.2.20-25), eq.2.44 is obtained. It must be noticed that the inertial terms due to the spacecraft velocity are considered through $\vec{g}$ and the accelerations because of the position are taken into account by $\vec{f_g}$.

$$\ddot{\vec{s}} = \ddot{\vec{r}}_c - \ddot{\vec{r}}_t = \vec{g}(\dot{\vec{r}}_c) - \vec{g}(\dot{\vec{r}}_t) + \vec{f_g}(\vec{r}_c) - \vec{f_g}(\vec{r}_t) \tag{2.44}$$

Rearranging this expression, it yields the following equation. In addition, it has been added a new acceleration term to account for the thrust force that the spacecraft can generate.

$$\ddot{\vec{s}} = \vec{g}(\dot{\vec{s}}) + \vec{f_g}(\vec{r}_c) - \vec{f_g}(\vec{r}_t) + \vec{a}_{Thrust} \tag{2.45}$$

Next step consists on expanding the above equation using a Taylor expansion.

$$\vec{f_g}(\vec{r}_c) = \vec{f_g}(\vec{r}_t) + \frac{\partial \vec{f_g}(\vec{r})}{\partial \vec{r}}|_{\vec{r}=\vec{r}_t} \cdot (\vec{r}_c - \vec{r}_t) \tag{2.46}$$

with Jacobian

$$M = \frac{\partial \vec{f_g}(\vec{r})}{\partial \vec{r}}|_{\vec{r}=\vec{r}_t} = \begin{bmatrix} \frac{\partial f_1}{\partial r_x} & \frac{\partial f_1}{\partial r_y} & \frac{\partial f_1}{\partial r_z} \\ \frac{\partial f_2}{\partial r_x} & \frac{\partial f_2}{\partial r_y} & \frac{\partial f_2}{\partial r_z} \\ \frac{\partial f_3}{\partial r_x} & \frac{\partial f_3}{\partial r_y} & \frac{\partial f_3}{\partial r_z} \end{bmatrix}_{r_t} = \begin{bmatrix} -\bar{U}_{xx} & -\bar{U}_{xy} & -\bar{U}_{xz} \\ -\bar{U}_{yx} & -\bar{U}_{yy} & -\bar{U}_{yz} \\ -\bar{U}_{zx} & -\bar{U}_{zy} & -\bar{U}_{zz} \end{bmatrix}_{r_t} \tag{2.47}$$

Introducing eq.2.46 into eq.2.45, the force terms depending on the chaser vehicle are cancel out. Written in vectorial form, the final equation would be:

$$\ddot{\vec{s}} = \vec{g}(\dot{\vec{s}}) + M \cdot \vec{s} + \vec{a}_{Thrust} \tag{2.48}$$

From the above expression, it is straightforwardly deduced the Relative Motion equations for the CRTBP. Notice that the partial derivatives terms are dependent on time, since the target position (r_t) changes as the vehicle moves. Nonetheless, these equations allow to investigate the chaser relative position by only knowing the target position through time, information which is aware of during a rendezvous manoeuvre.

$$\ddot{x} = 2\dot{y} - \bar{U}_{xx}|_{r_t}\, x - \bar{U}_{xy}|_{r_t}\, y - \bar{U}_{xz}|_{r_t}\, z + a_x \tag{2.49}$$
$$\ddot{y} = -2\dot{x} - \bar{U}_{yx}|_{r_t}\, x - \bar{U}_{yy}|_{r_t}\, y - \bar{U}_{yz}|_{r_t}\, z + a_y \tag{2.50}$$
$$\ddot{z} = -\bar{U}_{zx}|_{r_t}\, x - \bar{U}_{zy}|_{r_t}\, y - \bar{U}_{zz}|_{r_t}\, z + a_z \tag{2.51}$$

For completeness, the expressions for the second partial derivatives of the augmented gravitational potential are presented. They have been derived using the nomenclature used in the CRTBP equations of motion derivation. Please, note that x, y, z does not represent the relative distances as in eq.2.49-51; instead they are taken respect the Earth-Moon rotating reference frame. Then, the target position r_t must be referenced to that rotating reference frame when using the following expressions in the Relative Motion equations of motion.

$$\bar{U}_{xx} = 1 - \frac{1-\mu}{r_1^3} - \frac{\mu}{r_2^3} + \frac{3(1-\mu)(x+\mu)^2}{r_1^5} + \frac{3\mu[x-(1-\mu)]^2}{r_2^5} \tag{2.52}$$
$$\bar{U}_{xy} = \frac{3(1-\mu)(x+\mu)y}{r_1^5} + \frac{3\mu[x-(1-\mu)]y}{r_2^5} \tag{2.53}$$
$$\bar{U}_{xz} = \frac{3(1-\mu)(x+\mu)z}{r_1^5} + \frac{3\mu[x-(1-\mu)]z}{r_2^5} \tag{2.54}$$
$$\bar{U}_{yy} = 1 - \frac{1-\mu}{r_1^3} - \frac{\mu}{r_2^3} + \frac{3(1-\mu)y^2}{r_1^5} + \frac{3\mu y^2}{r_2^5} \tag{2.55}$$
$$\bar{U}_{yx} = \frac{3(1-\mu)(x+\mu)y}{r_1^5} + \frac{3\mu[x-(1-\mu)]y}{r_2^5} \tag{2.56}$$
$$\bar{U}_{yz} = \frac{3(1-\mu)yz}{r_1^5} + \frac{3\mu yz}{r_2^5} \tag{2.57}$$
$$\bar{U}_{zx} = \frac{3(1-\mu)(x+\mu)z}{r_1^5} + \frac{3\mu[x-(1-\mu)]z}{r_2^5} \tag{2.58}$$
$$\bar{U}_{zy} = \frac{3(1-\mu)yz}{r_1^5} + \frac{3\mu yz}{r_2^5} \tag{2.59}$$
$$\bar{U}_{zz} = -\frac{1-\mu}{r_1^3} - \frac{\mu}{r_2^3} + \frac{3(1-\mu)z^2}{r_1^5} + \frac{3\mu z^2}{r_2^5} \tag{2.60}$$

Chapter 3

Halo Orbits Dynamic Analysis

The presence of a second massive mass body in the CRTBP in comparison with the traditional Keplerian Two Body Problem results in a notably increase in the amount of available trajectory solutions. The appearance of some regions of equilibria in the system are an indication of the great impact of this second massive body. Exploring the new available possibilities for spacecraft trajectory design when considering the TBP has been always a field of study for astrodynamic scientists.

Although this study has been carried out over centuries, there were not discovered until the 1960s [10] that there were available orbits close to the equilibria or Lagrangian points. These orbits were called Halo orbit, since they appeared to be an halo encircling the moon when viewing from the Earth.

In this chapter, a detailed analysis of how it can be constructed this kind of orbits is presented. It comprehends both an analytical description of this kind of orbits, which aims to provide to the reader a deeper understanding about the physics responsible of producing them; and a numerical computation of such orbits for accurately describing their behaviour, so as to further meaningful analysis can be taken. In fact, developing the rendezvous problem, requires modelling the Halo orbit behaviour as close as possible to reality.

The second part of this chapter will be devoted to an analysis of the physical particularities of Halo orbits. This study comprehend a detailed stability analysis and the description of the spatial channels which are originated from these orbits, which are called Halo manifolds.

3.1 Equation of motion near the Libration points

Halo orbits are originated around the Lagrange points of the system. Therefore, moving the frame of reference to the Lagrange point whose Halo orbit is being investigated is useful for analytical describing the problem [11]. The change of coordinate is simply given by eq.3.1.

$$\hat{x} = \frac{x - 1 + \mu \pm \gamma}{\gamma}, \qquad \hat{y} = \frac{y}{\gamma}, \qquad \hat{z} = \frac{z}{\gamma} \tag{3.1}$$

This expression is particularly describing the coordinate change to L_1 (upper sign case) or L_2 (lower sign case) points. This transformation implies that in the new coordinate system, the variables are also scaled respect to the distance to the studied Lagrange point.

3.1.1 Expansion of the non linear equations

Development of the equations of motion using Legendre polynomial P_n results in a series of advantages when facing the CRTBP for the first time. It is particularly useful for obtaining approximate solutions of different orders of accuracy depending on the number of polynomial coefficients development. These equations are presented hereafter.

$$\ddot{x} - 2\dot{y} - (1 + 2c_2)x = \frac{\partial}{\partial x} \sum_{n \geq 3} c_n \rho^n P_n \left(\frac{x}{\rho} \right) \tag{3.2}$$

$$\ddot{y} + 2\dot{x} - (c_2 - 1)y = \frac{\partial}{\partial y} \sum_{n \geq 3} c_n \rho^n P_n \left(\frac{x}{\rho} \right) \tag{3.3}$$

$$\ddot{z} + c_2 z = \frac{\partial}{\partial y} \sum_{n \geq 3} c_n \rho^n P_n \left(\frac{x}{\rho} \right) \tag{3.4}$$

The coefficients of the precedent expansion are given by eq.3.5. Note that these coefficients are dependent on the mass parameter μ of the system and the Lagrange points which is being analyzed, which influence is introduced by the distance term (γ) explained in chapter 2.

$$c_n = \frac{1}{\gamma^3} \left((\pm)^n \mu + (-1)^n \frac{(1 - \mu)\gamma^{n+1}}{(1 \mp \gamma)^{n+1}} \right) \tag{3.5}$$

Based on these equations, it can be built the first approximations describing Halo orbit behaviour.

3.2 Halo orbits generation

Successive approximations are needed for a trustworthy representation of an Halo orbit. Furthermore, physical features of these orbits arise at each approximation stage.

3.2.1 Linear Approximation

Periodic solutions of the Linearized equations Investigating the linearized part of the expanded equations presented in eq.3.2-4, it can be deduced the existence of periodic solutions. Thus, the first evidences regarding the theoretical presence of Halo orbits arise at this step of the study.

$$\ddot{x} - 2\dot{y} - (1 + 2c_2)x = 0 \tag{3.6}$$
$$\ddot{y} + 2\dot{x} - (c_2 - 1)y = 0 \tag{3.7}$$
$$\ddot{z} + c_2 z = 0 \tag{3.8}$$

By simple exploration, it can be noticed that the out-of plane solution (z) corresponds to an harmonic oscillation, as long as the coefficient c_2 is greater than zero, which is totally uncoupled with the in-plane movement. On the contrary, the motion in the x-y plane is fully coupled. Then, by solving the characteristic equation belonging to the linearized equations, the information about the dynamic properties near the Lagrange points can be studied. Two imaginary and two real roots are obtained from the characteristic equation solution ($\pm\lambda, i \pm \omega$).

$$\lambda^2 = \frac{c_2 + \sqrt{9c_2^2 - 8c_2}}{2}, \qquad \omega_p^2 = \frac{2 - c_2 + \sqrt{9c_2^2 - 8c_2}}{2}, \qquad \omega_v^2 = c_2 \tag{3.9}$$

The two real solutions are opposite in sign, hence the solution for an arbitrary initial condition is expected to diverge with time. Nonetheless, restricting the initial condition in a manner such that only the convergent mode of the solution is excited, an unbounded solution can be obtained in the x-y plane.

Solution equations

The solution fulfilling the restrictions just mentioned will take the following form.

$$x = A_x cos(\omega_p t + \phi) \tag{3.10}$$
$$y = \kappa A_x sin(\omega_p t + \phi) \tag{3.11}$$
$$z = A_z(\omega_v t + \psi) \tag{3.12}$$

with

$$\kappa = \frac{\lambda^2 + 1 + 2c_2}{2\lambda} = \frac{2\lambda}{\lambda^2 + 1 - c_2} \tag{3.13}$$

This solution adjust to a periodic orbits as long as the ratio between the in-plane and the out-of-plane frequencies is not irrational, case in which a quasi-periodic solution would be obtained. Also, it is interesting to point out that restricting the solution to exist only in the x-y plane (it means, $z = 0$), the so-called Lissajous orbits [8] would be obtained instead of the Halo ones.

Amplitude Constraint Relationship

Applying a perturbation method as described in [9], it is found that the amplitudes in the x and z-axis are restricted by certain constraint. It is presented hereafter.

$$l_1 A_x^2 + l_2 A_z^2 + \Delta = 0 \tag{3.14}$$

l_1, l_2 and Δ coefficients of this expression depends on the Lagrange point whose Halo orbits are being analyzed. A detail explanation of how these values are calculated are presented in section 3.2.2.

Phase-Angle Relationship

It also exists a constraint equation relating the in-plane and out-plane phase angles for an Halo orbit, which is given in eq.3.15.

$$\psi - \phi = m\frac{\pi}{2} \quad m = 1,\ 3 \tag{3.15}$$

Two branches arise from this constraint, depending on the value of m. These branch on Halo orbits are going to be denoted as Class I & II, and they mainly

distinguish when the maximum amplitude of A_z occurs in the positive z-axis (which corresponds to $m = 1$) or in the negative part (when $m = 3$). An effect of this constraint is that both branches are mirror reflections of each other when viewed at the xy-plane, as it can be appreciated in Figure 3.1.

3.2.2 3rd Order Richardson Approximation

Expanding the non-linear equations using Legendre polynomial P_n allows to explore solutions with different orders of accuracy. 3^{rd} Order Richardson approximation for Halo orbits equations have been deduced [9] by using these expanded equations up to the order that gives name to the approximation. Then, the expanded equation would yield:

$$\ddot{x} - 2\dot{y} - (1 + 2c_2)x = \frac{2}{3}c_3(2x^2 - y^2 - z^2) + 2c_4x(2x^2 - 3y^2 - 3z^2) + O(4) \tag{3.16}$$

$$\ddot{y} + 2\dot{x} - (c_2 - 1)y = -3c_3xy - \frac{3}{2}c_4y(4x^2 - y^2 - z^2) + O(4) \tag{3.17}$$

$$\ddot{z} + c_2z = -3c_3xz - \frac{3}{2}c_4z(4x^2 - y^2 - z^2) + O(4) \tag{3.18}$$

Lindstedt-Poincaré Method

Lindstedt-Poincaré Method was used by [9] for developing the equation of the 3^{rd} Order Richardson approximation. For removing the secular terms that characterize this method, a new variable for considering time is introduced.

$$\tau = \nu t \tag{3.19}$$

where ν variable has been defined as:

$$\nu = 1 + \sum_{n\geq 1} \nu_n \qquad\qquad \nu_n < 1 \tag{3.20}$$

ν_n variable is of the order A_z^n and it has been selected in such a way the secular terms can be cancelled. Introducing the new time variable into eq.3.16-18 and properly selecting the values for the variable ν_n, most of the secular terms can be removed. That objective can be reached by using the following values of ν_n.

$$\nu_1 = 0, \qquad\qquad \nu_2 = s_1A_x^2 + s_2A_z^2 \tag{3.21}$$

Halo orbit 3rd order Approximation

After removing the secular terms applying Lindstedt-Poincaré Method, the 3^{rd} Order Richardson approximation for Halo orbits can be obtained.

$$\begin{aligned} x = {} & a_{21}A_x^2 + a_{22}A_z^2 - A_x cos(\tau_1) + (a_{23}A_x^2 - a_{24}A_z^2)cos(2\tau_1) + \\ & + (a_{31}A_x^3 - a_{32}A_x A_z^2)cos(3\tau_1) \end{aligned} \tag{3.22}$$

$$\begin{aligned} y = {} & \kappa A_x sin(\tau_1) + (b_{21}A_x^2 - b_{22}A_z^2)sin(2\tau_1) + \\ & + (b_{31}A_x^3 - b_{32}A_x A_z^2)sin(3\tau_1) \end{aligned} \tag{3.23}$$

$$\begin{aligned} z = {} & \delta_m A_z cos(\tau_1) + \delta_m d_{21} A_x A_z (cos(2\tau_1) - 3) + \\ & + \delta_m (d_{32}A_z A_x^2 - d_{31}A_z^3)cos(3\tau_1) \end{aligned} \tag{3.24}$$

where

$$\tau_1 = \omega_p \tau + \phi \tag{3.25}$$

$$\delta_m = 2 - m, \qquad m = 1, 3 \tag{3.26}$$

For the sake of clarity, all the coefficient involved in 3^{rd} Order Richardson approximation are listed hereafter.

$$a_{21} = \frac{3c_3(\kappa^2 - 2)}{4(1 + 2c_2)} \tag{3.27}$$

$$a_{22} = \frac{3c_3}{a(1 + 2c_2)} \tag{3.28}$$

$$a_{23} = -\frac{3c_3\lambda}{a\kappa d_1}\left[3\kappa^3\lambda - 6\kappa(\kappa - \lambda) + 4\right] \tag{3.29}$$

$$a_{24} = -\frac{3c_3\lambda}{4\kappa d_1}(2 + 3\kappa\lambda) \tag{3.30}$$

$$\begin{aligned} a_{31} = {} & -\frac{9\lambda}{4d_2}\left[4c_3(\kappa a_{23} - b_{21}) + \kappa c_4(4 + \kappa^2)\right] + \\ & + \left(\frac{9\lambda^2 + 1 - c_2}{2d_2}\right)\left[3c_3(2a_{23} - \kappa b_{21}) + c_4(2 + 3\kappa^2)\right] \end{aligned} \tag{3.31}$$

$$\begin{aligned} a_{32} = {} & -\frac{1}{d_2}\left\{\frac{9\lambda}{d_2}\left[4c_3(2a_{23} - \kappa b_{21}) + \kappa c_4\right]\right\} - \\ & - \frac{1}{d_2}\left\{\frac{3}{2}(9\lambda^2 + 1 - c_2)\left[c_3(\kappa b_{22} + d_{21} - a_{24}) - c_4\right]\right\} \end{aligned} \tag{3.32}$$

$$b_{21} = -\frac{3c_3\lambda}{2d_1}(3\kappa\lambda - 4) \tag{3.33}$$

$$b_{22} = \frac{3c_3\lambda}{d_1} \tag{3.34}$$

$$\begin{aligned} b_{31} =& \frac{3}{8d_2}\left\{8\lambda[3c_3(\kappa b_{21} - 2a_{23}) - c_4(4+\kappa^2)]\right\} + \\ &+ \frac{3}{8d_2}\left\{(9\lambda^2 + 1 + 2c_2)[4c_3(\kappa a_{23} - b_{21}) + \kappa c_4(4+\kappa^2)]\right\} \end{aligned} \tag{3.35}$$

$$\begin{aligned} b_{32} =& \frac{1}{d_2}\left\{9\lambda[c_3(\kappa b_{22} + d_{21} - 2a_{24}) - c_4]\right\} + \\ &+ \frac{1}{d_2}\left\{\frac{3}{8}\left(9\lambda^2 + 1 + 2c_2\right)[4c_3(\kappa a_{24} - b_{22}) + \kappa c_4]\right\} \end{aligned} \tag{3.36}$$

$$d_{21} = -\frac{c_3}{2\lambda^2} \tag{3.37}$$

$$d_{31} = \frac{3}{64\lambda^2}(4c_3a_{24} + c_4) \tag{3.38}$$

$$d_{32} = \frac{3}{64\lambda^2}[4c_3(a_{23} - d_{21}) + c_4(4+\kappa^2)] \tag{3.39}$$

where d_1 and d_2 from these coefficient correspond to:

$$d_1 = \frac{3\lambda^2}{\kappa}[\kappa(6\lambda^2 - 1) - 2\lambda] \tag{3.40}$$

$$d_2 = \frac{8\lambda^2}{\kappa}[\kappa(11\lambda^2 - 1) - 2\lambda] \tag{3.41}$$

Third Order Richardson approximation also has to fulfil the constraints previously defined: both the amplitude constraint relationship given by eq.3.14 and the phase-angle relationship stated in eq.3.15. The coefficients for those constraints can be calculated by using the following equations.

$$l_1 = -\frac{3}{2}c_3(2a_{21} + a_{23} + 5d_{21}) - \frac{3}{8}c_4(12 - \kappa^2) + 2\lambda^2 s_1 \tag{3.42}$$

$$l_2 = \frac{3}{2}c_3(a_{24} - 2a_{22}) + \frac{9}{8}c_4 + 2\lambda^2 s_2 \tag{3.43}$$

Hereafter, it is depicted an example of the two solution branches of an Halo orbit calculated by following 3^{rd} Order Richardson approximation. Notice that this result is what is obtained once the backward transform to the general coordinate frame (the rotating one defined in Chapter 3) is performed.

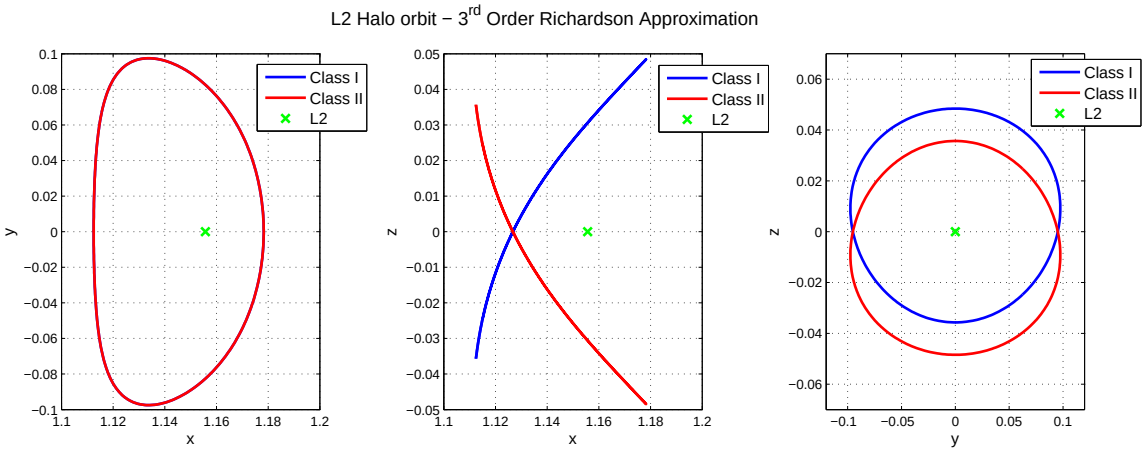

Figure 3.1: 3^{rd} Order Approx. L_2 Halo orbits with opposite direction of rotation example.

3.2.3 Numerical Halo Generation

Up to now, successive approximation from the original CRTBP equations of motion have been done for investigating the periodic orbits originated at Lagrange points proximity. Nonetheless, they are not as representative to reality than directly using the general equation of motion. Hence, for achieving a realistic representation of those orbits during the rendezvous analysis that is going to be done in the next chapter, a numerical method for generating Halo orbits must be provided. [12] [13] [14]

State Transition Matrix

Before entering in the numerical method details, it must be understood the concept of State Transition Matrix (STM). The STM is matrix which allows to reference a nearby trajectory to a given one when the motion is subject to a non-linear set of differential equations. Therefore, it allow to investigate the vicinity solutions of a defined trajectory.

For a trajectory in the CRTBP, the STM during the trajectory can be calculated by propagating in time the following 36 differential equations of motion. Written in matrix form, it yields:

$$\dot{\Phi}(t, t_0) = Df(x)\Phi(t, t_0) \tag{3.44}$$

where

$$Df(x) = \begin{bmatrix} 0 & 0 & 0 & 1 & 0 & 0 \\ 0 & 0 & 0 & 0 & 1 & 0 \\ 0 & 0 & 0 & 0 & 0 & 1 \\ -\bar{U}_{xx} & -\bar{U}_{xy} & -\bar{U}_{xz} & 0 & 2 & 0 \\ -\bar{U}_{yx} & -\bar{U}_{yy} & -\bar{U}_{yz} & -2 & 0 & 0 \\ -\bar{U}_{zx} & -\bar{U}_{zy} & -\bar{U}_{zz} & 0 & 0 & 0 \end{bmatrix} \tag{3.45}$$

So as to refer the calculated STM to a particular trajectory, it is evident that the initial condition would be $\Phi(t_0, t_0) = I_6$, where I_6 is an identity matrix of dimension 6.

The shooting method

The shooting method is a numerical method that correct the given trajectory by comparing it with the target one and making some corrections until a match between both trajectories is attained.

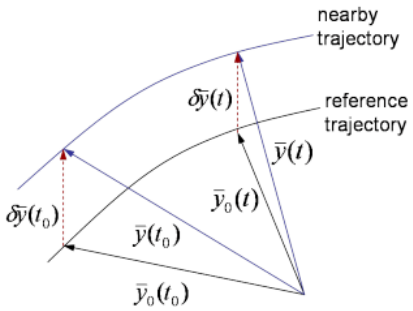

Figure 3.2: Reference and nearby trajectories relation.

According to Halo orbit properties, it is known that when the orbit crosses the x-z plane ($y = 0$), the x and z velocity components are zero. Then, the initial vector for an Halo orbit will take the form:

$$X(t = 0) = [x_0, 0, z_0, 0, v_{y0}, 0] \tag{3.46}$$

It is not necessary to propagate the whole of the orbit for finding it. Instead, the symmetry property of an orbit can be used for reducing the time of

propagation to one half the orbit period. Then, the final condition ensuring that an orbit has been found would be:

$$X(t = T/2) = [x_d, 0, z_d, 0, v_d, 0] \tag{3.47}$$

Since the initial propagation would no result in the desired in the first trial, a correction process has to be followed to correct the initial conditions by using a differential correction term.

$$X(t = 0)_{i+1} = [x_0, 0, z_0, 0, v_{y0}, 0]_i + [\partial x_0, 0, \partial z_0, 0, \partial v_{y0}, 0]_i \tag{3.48}$$

Differential variational equations are used for calculating those differential terms at every iteration i.

$$\delta\bar{x} = \Phi(T/2, 0)\delta\bar{x}_0 + \frac{\partial\bar{x}}{\partial t}\delta(T/2) \tag{3.49}$$

where $\bar{x}$ is the state vector

$$\bar{x} = [x, y, z, v_x, v_y, v_z]^T \tag{3.50}$$

For clarity purposes, the STM terms used next is going to be expressed as it is shown in eq.3.48.

$$\begin{bmatrix} \partial x_f \\ \partial y_f \\ \partial z_f \\ \partial v_{x,f} \\ \partial v_{y,f} \\ \partial v_{z,f} \end{bmatrix} = \begin{bmatrix} \Phi_{11} & \Phi_{12} & \Phi_{13} & \Phi_{14} & \Phi_{15} & \Phi_{16} \\ \Phi_{21} & \Phi_{22} & \Phi_{23} & \Phi_{24} & \Phi_{25} & \Phi_{26} \\ \Phi_{31} & \Phi_{32} & \Phi_{33} & \Phi_{34} & \Phi_{35} & \Phi_{36} \\ \Phi_{41} & \Phi_{42} & \Phi_{43} & \Phi_{44} & \Phi_{45} & \Phi_{46} \\ \Phi_{51} & \Phi_{52} & \Phi_{53} & \Phi_{54} & \Phi_{55} & \Phi_{56} \\ \Phi_{61} & \Phi_{62} & \Phi_{63} & \Phi_{64} & \Phi_{65} & \Phi_{66} \end{bmatrix} \begin{bmatrix} \partial x_0 \\ \partial y_0 \\ \partial z_0 \\ \partial v_{x,0} \\ \partial v_{y,0} \\ \partial v_{z,0} \end{bmatrix} \tag{3.51}$$

Regarding to eq.3.49, the unknown variable is the initial differential term $\partial\bar{x}_0$. Notice that the final differential term $\partial\bar{x}$ can be calculated taking the difference between the target final point and the one obtained during the trial trajectory propagation.

$$\partial\bar{x} = [x_d, 0, z_d, 0, v_d, 0] - [x_{f,i}, 0, z_{f,i}, 0, v_{f,i}, 0] \tag{3.52}$$

Then, relationships between the terms relevant in this orbit search can be derived. Following this procedure allows to avoid inverting the complete STM matrix when calculating the initial differential terms, thus reducing a lot of the computational time due to this method.

Depending on which of the initial terms of the initial vector is fixed, two different formula are needed. If z_0 is wanted to remain constant through the shooting method calculation:

$$\begin{bmatrix} \partial v_{x,f} \\ \partial v_{z,f} \end{bmatrix} = \left\{ \begin{bmatrix} \Phi_{41} & \Phi_{45} \\ \Phi_{61} & \Phi_{65} \end{bmatrix} - \frac{1}{\dot{y}} \begin{bmatrix} \ddot{x} \\ \ddot{z} \end{bmatrix} \begin{bmatrix} \Phi_{21} & \Phi_{25} \end{bmatrix} \right\} \begin{bmatrix} \partial x_0 \\ \partial \dot{y}_0 \end{bmatrix} \tag{3.53}$$

On the contrary, if z_0 is wanted to be kept fixed:

$$\begin{bmatrix} \partial v_{x,f} \\ \partial v_{z,f} \end{bmatrix} = \left\{ \begin{bmatrix} \Phi_{43} & \Phi_{45} \\ \Phi_{63} & \Phi_{65} \end{bmatrix} - \frac{1}{\dot{y}} \begin{bmatrix} \ddot{x} \\ \ddot{z} \end{bmatrix} \begin{bmatrix} \Phi_{23} & \Phi_{25} \end{bmatrix} \right\} \begin{bmatrix} \partial z_0 \\ \partial \dot{y}_0 \end{bmatrix} \tag{3.54}$$

Choosing an option among the other is just a decision about what vicinity of Halo solutions is preferred to explore when the initial guess condition is explored.

As any shooting finder method, an appropriate selection of the initial guess is necessary to ensure convergence in the solution. Thus, 3^{rd} Order Richardson Approximation has been used as initial guess, since this expression can be derived analytical and it is expected to be adjusted enough to reality.

	3rd O.R.	Numerical
x_0	1.1124550077766104	1.1107336309849527
y_0	0	0
z_0	0.035680331960522345	0.035698470121507432
v_{x0}	0.0001677345614018	0
v_{y0}	0.20156708661850475	0.20366491366860792
v_{z0}	-0.0010217302462787591	0

Table 3.1: L_2 Halo orbit IC numerical computation using single shooting differential correction.

It can be appreciated in Table 3.1 that, as expected, 3^{rd} order Richardson approximation provides an appropriate initial guess trajectory for the computation of the numerical Halo orbit. Indeed, convergence of the shooting method rapidly arises thanks to that fact. For the shown solution, 15 iterations have been needed until the numerical orbit was successfuly calculated with a tolerance error of 10^{-15}.

A graphical representation of both the approximated and the numerical halo orbits is despicted next. Note that although both seems to be nearly equal, only the numerical one is obtained through a propagation of the CRTBP differential equations of motion. In fact, due to the deterministic chaos associated to the CRTBP, propagating the differential equations of motion using as initial condition the values from the 3^{rd} Order Richardson Approximation would yield in an completely unbounded solution.

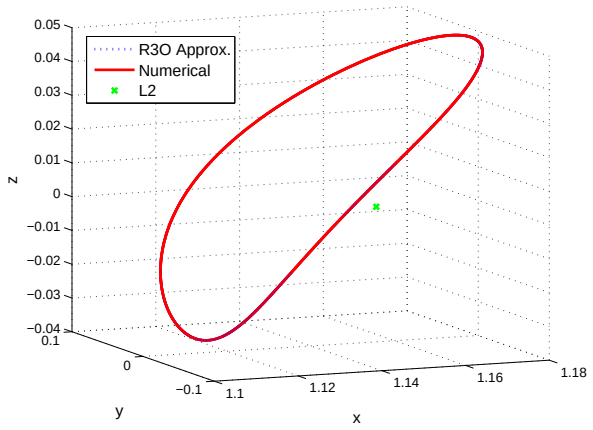

Figure 3.3: Comparison of approximated vs numerically calculated Halo orbit

3.3 Dynamic Analysis

Once the finding and successful computation of the Halo orbits originated close to the L_1 and L_2 libration points have been reached, the natural dynamic behaviour from those are going to be studied. Gaining a extensive comprehension of the particular dynamic properties for such orbit let the space mission designers familiarize with the fuel consumption that those orbits will cost (depending on how stable the orbits would be) and understand what set of trajectories might be appropriate for fulfilling their objectives when travelling to those orbits.

3.3.1 Halo Orbit Stability

Stability of periodic orbits is studied by analyzing the monodromy matrix corresponding to that orbit. The eigenvalues solution of such matrix, which are named as Floquet multipliers or characteristic multipliers, contain all the stability information regarding the phase space in the vicinity of the orbit. The solution space of this eigenvalue problem can be decomposed in three different types of subspace.

- *The Stable Subspace.* A particle departing from this subspace will return to the original orbit trajectory. It corresponds to eigenvalues magnitudes lower than 1.
- *The Unstable Subspace.* Moving along this subspace direction will imply that a particle will diverge from the orbit as long as time advances. This subspace corresponds to eigenvalues magnitudes greater than 1.
- *The Center subspace.* It correspond to the subspace at which the solution is marginally stable, thus a particle left in that subspace would remain there.

This subspace can be found by calculating the eigenvectors associated to the eigenvalues of the monodromy matrix.

Monodromy Matrix

The Monodromy Matrix is the STM corresponding to one period of integration from an orbital point. By using different properties of the STM, it can be avoided the STM propagation over one period. STM is simplectic, thus it fulfills these two relations [15].

$$\Phi(t_2, t_0) = \Phi(t_2, t_1)\Phi(t_1, t_0) \tag{3.55}$$

$$\Phi(t_1, t_0) = \Phi^{-1}(t_1, t_0) \tag{3.56}$$

Using this properties, an expression for calculating the monodromy matrix can be obtained. In this case, the STM is only necessary to be integrated over half a period, which helps reducing errors associated to the numerical integration scheme which would be used.

$$\Phi(T, 0) = G \begin{bmatrix} 0 & -I \\ I & -2\Omega \end{bmatrix} \Phi^T(T/2, 0) \begin{bmatrix} -2\Omega & I \\ -I & 0 \end{bmatrix} G\Phi(T/2, 0) \tag{3.57}$$

where

$$G = \begin{bmatrix} 1 & 0 & 0 & 0 & 0 & 0 \\ 0 & -1 & 0 & 0 & 0 & 0 \\ 0 & 0 & 1 & 0 & 0 & 0 \\ 0 & 0 & 0 & -1 & 0 & 0 \\ 0 & 0 & 0 & 0 & 1 & 0 \\ 0 & 0 & 0 & 0 & 0 & -1 \end{bmatrix} \qquad \Omega = \begin{bmatrix} 0 & 1 & 0 \\ -1 & 0 & 0 \\ 0 & 0 & 0 \end{bmatrix} \tag{3.58}$$

Stability of L1 and L2 Halo orbits

Solutions corresponding to the three subspaces mentioned before has been found for L_1 and L_2 Halo orbits. It can be observed in Figures 3.4-5 how pushing a point particle through the unstable subspace it rapidly diverges from the orbit whilst pushing a particle through the stable one results in a quick convergence with the original orbital period solution.

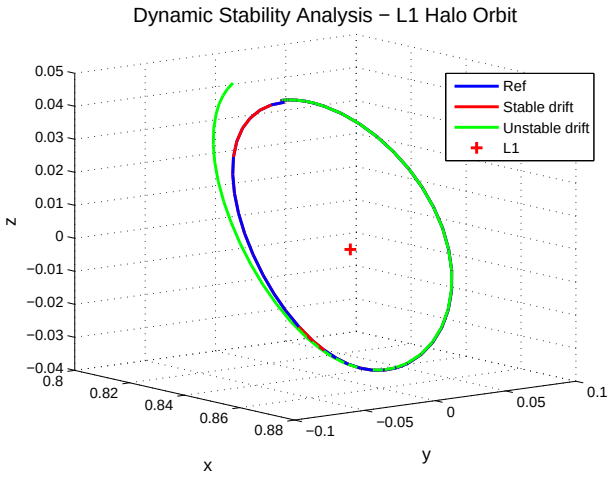

Figure 3.4: L_1 Halo orbit stability analysis.

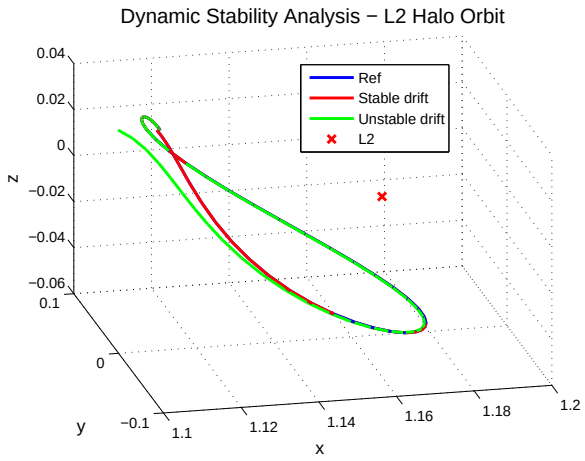

Figure 3.5: L_2 Halo orbit stability analysis.

From this analysis, it can be deduced that this orbits are useful to be used in space missions as long as it is control that the spacecraft do not enter in the unstable subspace of the orbit. However, from the six eigenvalues solution there is only one unstable, hence avoiding it should not a huge challenge.

3.3.2 Halo Manifolds

There are some positions in the CRTBP at which if a spacecraft is placed at the right velocity, the Halo orbit can be reached without the necesity os spending any amount of propellant. It also exists a set of trajectories which allows the opposite travel, it means, very far positions can be reached from an Halo orbit without any propellant consumption. These trajectories are known as Halo Manifolds. The first of described trajectories are referred as stable manifolds, since they carry the particles on it to an Halo orbit whilst the another one receives the name of unstable manifold.

According to [16][17], manifolds are tangent to the linear eigenvector direction of a given Halo orbit. Then, these manifolds can be calculated by following the next procedure.

For a given Halo orbit, the eigenvector solutions for each of the points conforming the orbit are calculated. Then, a shift of the Halo orbit points in the direction of their corresponding eigenvector yields in an excitation of the modes of the eigenvalues associated to such eigenvector. Stable and unstable manifolds are the focus of interest in this study, so the eigenvector referred to those phase space properties must be selected. This shift is done according to eq.3.59.

$$\vec{x}_{Mani,0} = \vec{x}^{\,*} \pm d\xi_n \tag{3.59}$$

At this stage, the distance drift between both the original Halo orbit and the Halo manifold can be controlled when they are being calculated. Stable manifolds are then obtained by integrating backward in time the equations using as starting condition the point obtained in eq.3.59. For the unstable halo manifolds calculation, the same procedure must be followed but the integration must be done forward in time.

L1 Halo Manifolds

The halo manifolds for a L_2 Halo orbit have been generated. A drift of $50\,km$ has been left between the original Halo orbit and the manifolds in this calculation. In Figure 3.7, a graphical representation of these manifolds is depicted. It can be observed that natural trajectories for going from Earth to the halo or vice-versa; or for travelling from the halo to the Moon exist in the CRTBP phase space. In fact, those solutions (stable versus unstable) are symmetrical.

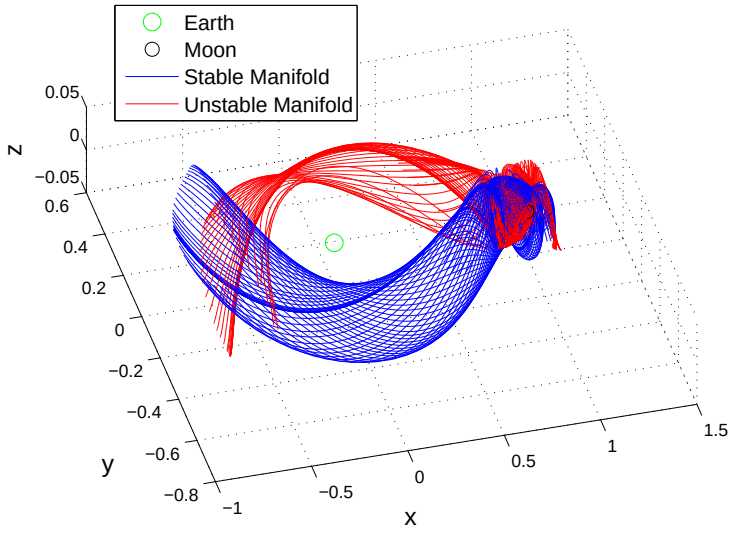

Figure 3.6: 3D representation of the stable and unstable L_1 Halo manifolds

In order to get a better understanding of the shape of those manifolds, the following figure is presented. The halo manifold and its associated L_1 Halo points from which they take origin can clearly be viewed by this 2D perspective.

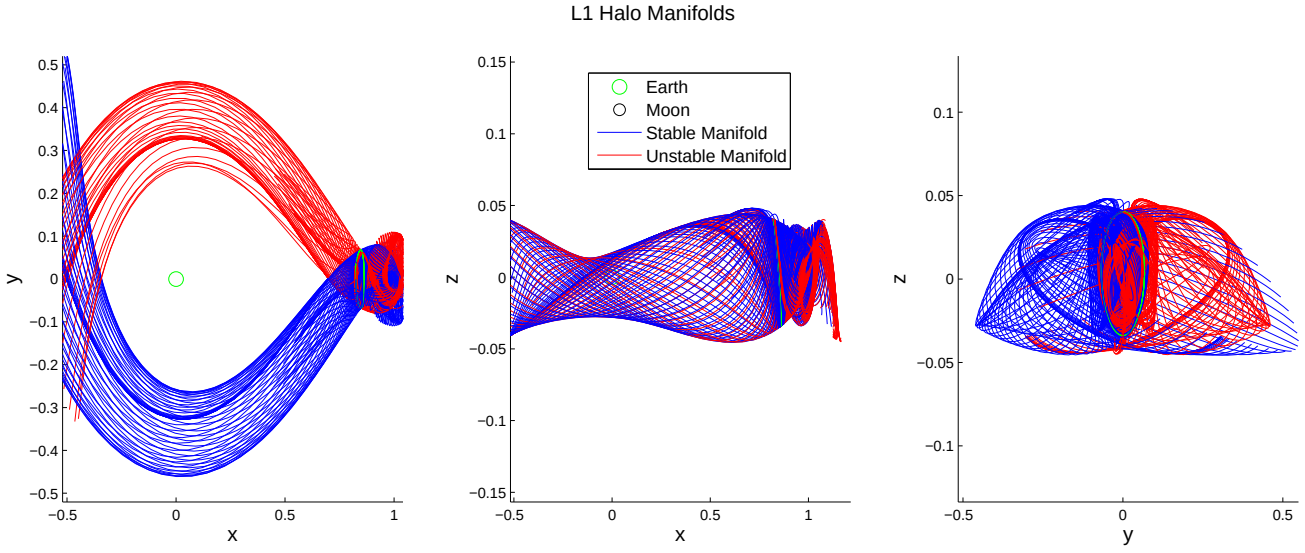

Figure 3.7: 2D representation of L_1 Halo manifolds

L2 Halo Manifolds

Studying the halo manifolds from a L_2, similar conclusion to the ones for the L_1 halo manifolds arises. Nonetheless, the dimensional shape of those spatial structural are quite different. Looking at Figures 3.8, it can be observed that as opposed to L_1 halo manifolds, there exists some L_2 manifolds which move so far from the Earth and the Moon system. A better insight of this conclusion can be obtained in Figure 3.9, where it has been zoomed out the solution shown in Figure 3.8. With the sake of clearness, only the stable orbit has been drawn, taken advantage of the fact that both results are symmetric.

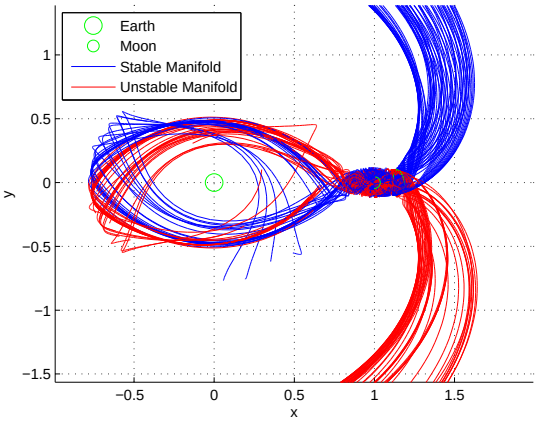

Figure 3.8: 3D L_2 Halo manifolds (zoomed view).

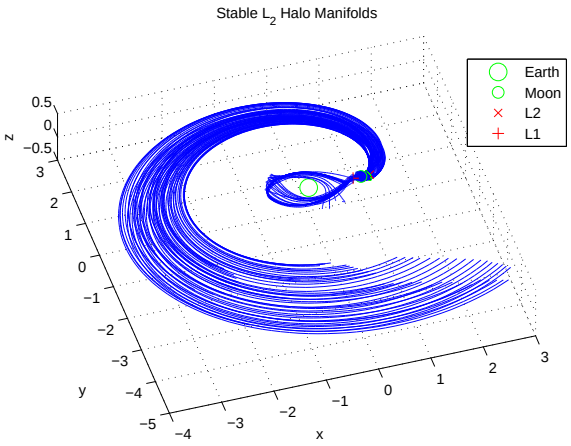

Figure 3.9: Orbit injection L_2 Halo manifolds

This result can have a greatly effect when selecting some orbits for future in-space missions. In fact, L_2 has shown to proportionate some space channels along which an spacecraft can enter into deep space (using the appropriate unstable manifolds) or return to the Earth-Moon system (by following the correct stable manifold).

Furthermore, as in the case of the L_1 halo manifolds, there are manifolds trajectories with destinations close to Earth or the Moon. Thus, this kind of orbit also offers a no-fuel scape to a moon base or to Earth in case of an emergency arises during a mission. Hence, these kind of orbits collect all the characteristics than a spacial base of operation for in-space mission should have. A detailed view of how these manifolds would intersect with their Halo of origin is depicted in Figure 3.10.

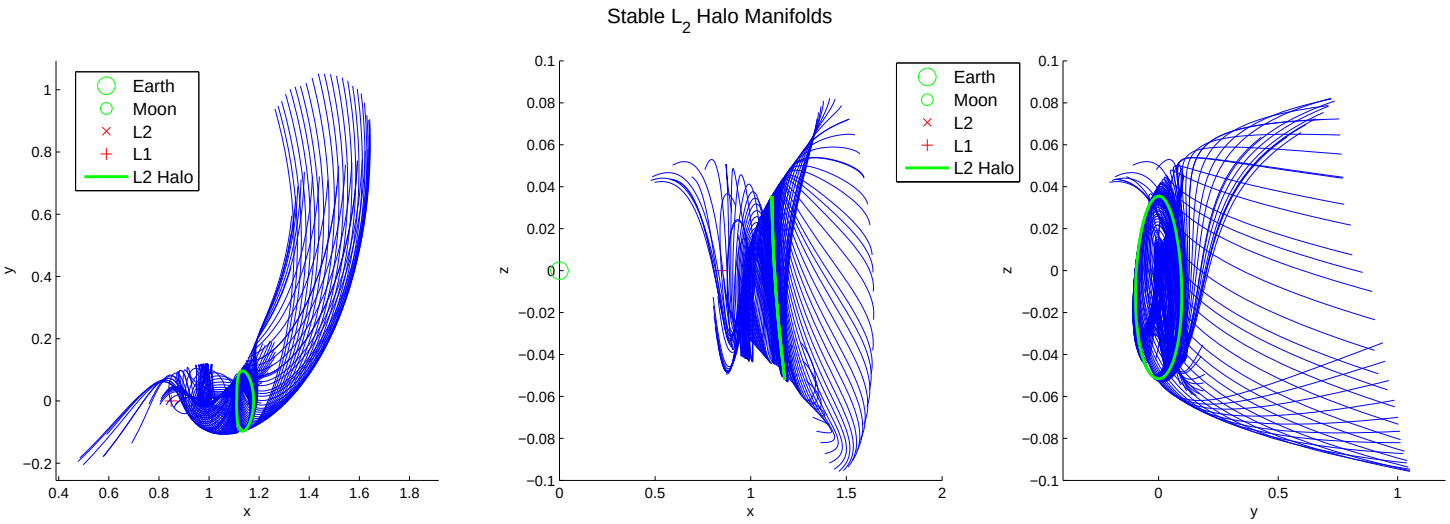

Figure 3.10: 2D L_2 Halo manifolds

3.4 Near Rectilinear Orbit: A special kind of Halo

Between L_1 and L_2 Halo orbits, it has been discovered that another non-keplerian type of orbits exists. These orbits are known with the name of Near Rectilinear Orbits (NRO), since when viewed from the x-z plane, the seems to be almost rectilinear.

NRO finding and implementation

The shooting method described for the Halo computation has also been used for searching this kind of orbits. In this case, since this orbits are known to be originated close to the Moon, eq.3.54 has been used, so that the value of the x_0 position is kept fixed. Then, for providing the initial condition for that method, L_2 halo orbits with increased A_z values have been investigated using the 3^{rd} Order Richardson Approximation with that purpose. Some examples showing the procedure just described are presented in Table 3.1.

	x_0	z_0	$v_{y,0}$	T_{ad}
NRO	1.011035058800000	-0.172905309010342	-0.077984100864307	1.360808650588530
L2 Halo 1	1.073928204515193	0.069009838196433	0.305190130805224	3.280248154641079
L2 Halo 2	1.095225264653613	0.055019962805025	0.246781601949166	3.352056621275708
L2 Halo 3	1.110743987357903	0.035680331960522	0.203635656950066	3.415528773516606

Table 3.2: NRO of the L2 Halo orbits family.

By graphically representing these results, the differences between L_2 Halo orbits and NRO gets clearer. In addition, it can be clearly observed how the NRO almost follow a straight line in the z-axis.

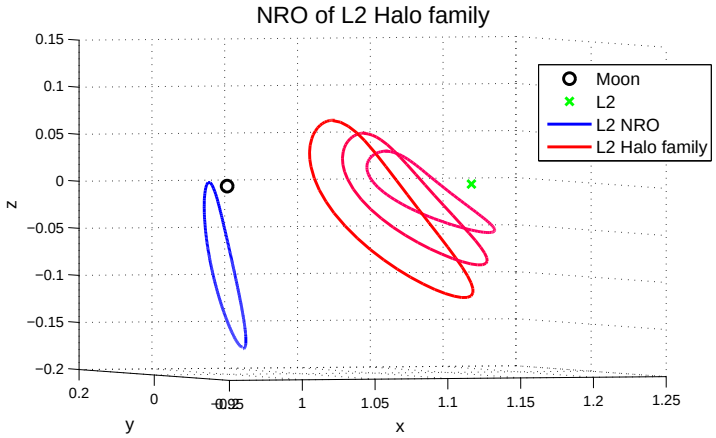

Figure 3.11: Near Rectilinear Orbit (NRO).

Stability Analysis

For the found NRO, it has been noticed to be very stable, since the unstable manifolds yields in a non very much unbounded solution. Nonetheless, considering the competitive features for in-space mission described before for the L_2 Halo orbit, L_2 Halo orbits offer higher advantages.

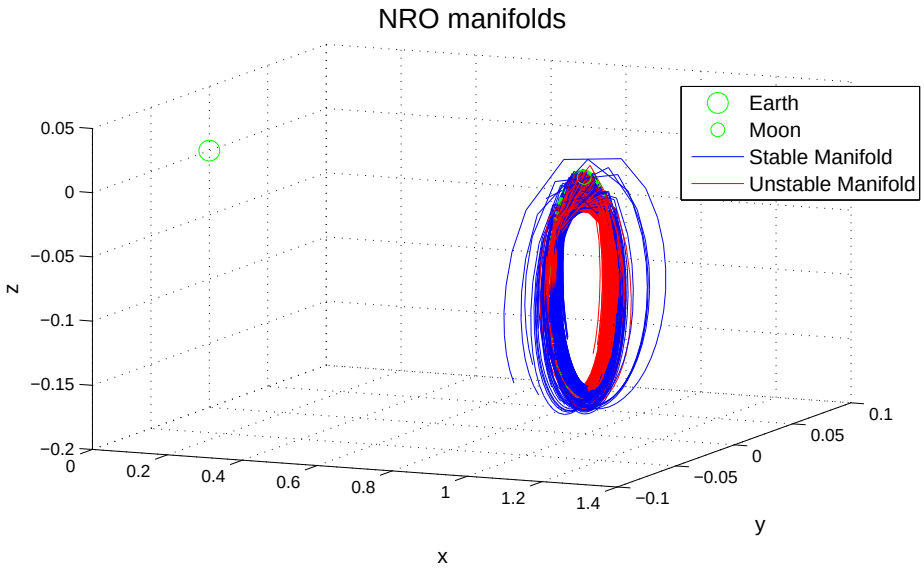

Figure 3.12: NRO Manifolds.

Chapter 4

Rendezvous Problem

Rendezvous at space is a mission that have been undertaken from the space exploration commences. The necessity of providing support or simply reaching a target destiny has aimed the study of this problem along these years. Nonetheless, up to now space rendezvous and docking have been carried out in the well-known Keplerian orbits. On the other hand, technology maturity has been greatly evolved during the recent times, which has considerably broaden the space mission capabilities. The appearance of the Electric Propulsion is a noted example of this maturity, being their high Specific Impulse (I_{sp}) one of the leading features letting that new demanding space missions are available.

This technology maturity and the appearance of new missions has lead to begin investigating new interesting kind of orbits which can be able to carry out the upcoming space missions. Particularly, recent studies has shown [2] that some Non-Keplerian orbits such as Halo Orbits or Near Rectilinear ones can offer for some missions some advantages respect to the traditional ones. As consequence, it is being noticed that making spacecraft rendezvous at such orbits can be a leading opportunity to explore.

Throughout this chapter, it is going to deeply analyzed this problem: the spacecraft rendezvous in Non-Keplerian orbits. Due to the wide variety of different options which are present in this problem, a general problem case has been defined in such a way that it describes any possible problem in this field.

4.1 Problem Description

The general rendezvous problem can be defined as the mission of intercepting a target vehicle at a specific location and time instant departing from an arbitrary position. Thus, optimizing this rendezvous manoeuvre is the main objective of this chapter. Settling the problem on a space environment, it comes out that the most universal initial departure position for a space mission is a point located at its parking orbit. This thesis is not focused in the optimization of prior manoeuvres, concretely the spacecraft insertion in the parking orbit, since this analysis is well known in the literature [18] and generally it yields to the selection of an appropriate launcher which allows to reach the desired parking orbit at the minimum cost possible.

According the exposed reasons, the problem of study consists on the optimization of the trajectory making rendezvous of a spacecraft orbiting in an Halo orbit from the initial Earth parking orbit. This problem must be particularize in order to be able to extract useful information about the rendezvous problem. The particularities of the case of study are accomplished hereafter.

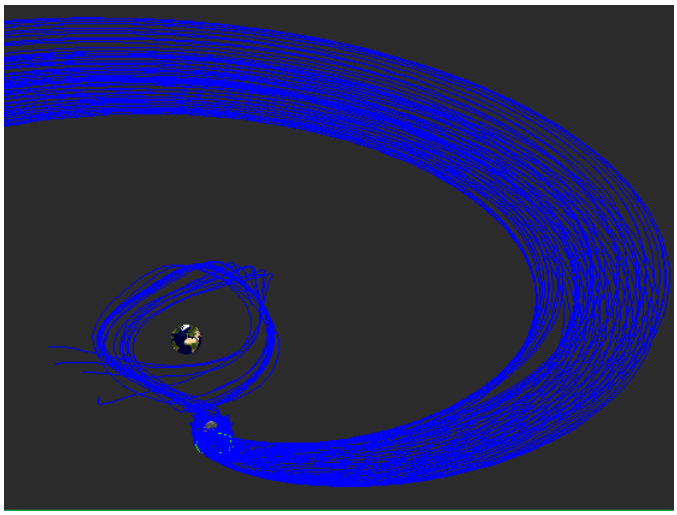

Figure 4.1: Halo manifolds reaching a target L_2 Halo orbit.

The target spacecraft is assumed to be an Halo orbit belonging to the L_2 Lagrangian point. This orbit have been noticed to have new favourings features for future space missions, as it has been throughout explained in chapter 1. For this reason, it has been chosen in contrast to the other ones originated in the remaining Lagrange points. Then, the chaser departure position must be defined. By considering the Halo orbits dynamic properties

studied in Chapter 3, it has been realized that Halo manifolds are some kind of spatial channels connecting some points of the CRTBP system with Halo orbits. Therefore, it quickly comes to mind that using these manifolds will let highly reduce the fuel cost of the rendezvous mission. Then, it has been assumed that the parking orbit connects with one of the manifold trajectories arriving to the target L_2 Halo orbit.

In order to make this problem as general as possible, it has been also assumed that the final orbit is not directly achieved by following the Halo manifold. This orbit will be also a L_2 halo orbit, but with different amplitude. In this way, typical trajectory deviation errors of real missions can be modelled in certain way.

Then, the rendezvous mission can be divided in three submissions: the Halo manifold insertion up to reaching an Halo orbit close to the target one, the transfer from this Halo orbit to the desired one and ultimately, the rendezvous in the target Halo orbit. A detailed description of each of these submissions is provided so as to gain knowledge about their individual impact in the complete rendezvous mission.

4.2 Analysis Cases

Each one of the cases subdividing the general rendezvous problem present specific features.

4.2.1 Halo Manifold travel

This manoeuvre consists on keeping the spacecraft into the stable manifold of the target orbit. The point at which insertion is made has been selected to be at the Halo manifold passing closest to the Earth. Thus, the parking orbit has been assumed to cross this departure point. Recall that the launcher is supposed to carry the spacecraft to the target parking orbit and inserting it in the desired Halo manifold. In this way, the optimal control problem can focus in the analysis of the proper departure point. The reference point fulfilling the mentioned criteria has been defined to be:

$$x_0 = -0.158936603538961 \qquad v_{x,0} = 1.131338323385016$$

$$y_0 = -0.442281426413653 \qquad v_{y,0} = -0.206724217341139$$

$$z_0 = -0.017997726224347 \qquad v_{z,0} = 0.106963329480634$$

The final arrival point has been located to be at an L_2 Halo orbit with amplitude of around 95000 km. Halo manifolds calculation has been taken with a 50 km drift from the target L_2 Halo orbit (with amplitude of around 95000km), so the destination point from this Halo is expected to be belonging or very close to the Halo manifold. The destination state vector, in the rotating reference frame, has taken the values specified next. Note that not only the position is wanted to be reached. In fact, attaining the correct velocity at this point is extremely important so as to ensure that the spacecraft will follow the desired Halo just after finishing the manoeuvre.

$$x_f = 1.110733630984952 \qquad v_{x,f} = 0$$

$$y_f = 0 \qquad v_{y,f} = 0.203664913668611$$

$$z_f = 0.035698470121507 \qquad v_{z,f} = 0$$

4.2.2 Transfer from a near Halo orbit

The next manoeuvre consists on travelling from the transition Halo orbit to the target one. This study case aims to get a deep analysis of the departure and final positions which are more optimum for making the transfer. In addition, it is also pretended to analyze the cost penalty incurred due to injecting the vehicle in an orbit close to the target one.

With this purpose, many different optimal control problems will be taken considering either different departure points (from the transition Halo orbit) and distinct points (of the target Halo orbit).

4.2.3 Rendezvous in the target Halo orbit

The last manoeuvre consists on making a final rendezvous manoeuvre when both the target and the chaser spacecraft are orbiting at the same Halo orbit. In this case of analysis, the chaser vehicle needs to speed up or slow down in order to catch de target. This manoeuvre is analyzed by introducing as initial condition of the problem the shift in time that separates the chaser from the target.

On the other hand, this analysis case is also useful for analyzing the cost in terms of fuel due to the final time drift between both analyzed vehicles when the chaser arrives the final Halo orbit. In reality, it is possible that small deviations from the designed rendezvous trajectory to meet the rendezvous

mission occurs. Thus, it will result that in the final orbit would be a phase drift between the vehicles. For such cases, this analysis can be also used.

4.3 Numerical Implementation

Optimal control theory concepts knowledge are requested prior to starting the numerical implementation of the study cases defined before. Expressing a control problem into a correct mathematical formulation are crucial for lately using any program solver to find the solution of the optimal control problem. [19][20]

4.3.1 Mathematical description of the problem

Consider a general optimal control problem case [21]. It would be expressed in terms of an objective function which is intended to minimize (J), which is subject to a set of constraints.

$$J = \Phi\left(x_f, t(x_f)\right) + \int_{t_0}^{t_f} L\left(x(t), u(t), t\right) \tag{4.1}$$

Commonly, any optimal control problem is subject to three different types of constraints: the system governing equations (eq.4.2), which account for the motion laws governing the vehicle motion; the path constraints (eq.4.3), expressing relations between the system variables and their values constraint (i.e., considering a mass model of an arbitrary system, this constraint is used for limiting the mass values to the positive ones since otherwise they are totally senseless); and the terminal constrains (eq.4.4), indicating the desired final conditions for the vehicle state vector. It must be noticed that $\mathbf{x}$ is the state vector of the problem and $\mathbf{u}$ is the control variable.

$$\dot{\mathbf{x}}(t) = \mathbf{f}\left(\mathbf{x}(t), \mathbf{u}(t), t\right), \quad t_0 < t < t_f \tag{4.2}$$

$$\mathbf{g}(\mathbf{x}, \mathbf{u}, t) \leq 0, \quad t_0 < t < t_f \tag{4.3}$$

$$\Psi(\mathbf{x}(t_f), t_f) = 0 \tag{4.4}$$

The rendezvous problem previously stated perfectly adjusts to this optimal control problem definition. Hence, these presented equations are going to be particularized for that problem, but firstly, it must be defined the state and control variables for the rendezvous problem.

- The state vector **x**. For the study case, the state vector are the six variables that completely define the spacecraft motion in the CRTBP. These are the spacecraft position and its velocity with respect to the rotating reference frame. $\mathbf{x} = [x, y, z, \dot{x}, \dot{y}, \dot{z}]$.

- The control vector **u**. The variable which can be control in a spacecraft is the thrust. Since the thrust is proportional to the acceleration, this last variable will be the one used as the control variable.

Objective function definition

The main goal of any space mission is minimizing the amount of fuel consumption through it, since it will results in an increase of the mission capability. Fuel consumption is directly related to the thrust usage along the mission, as the rocket equation denotes:

$$F_{Thrust} = \dot{m} \cdot I_{sp} \tag{4.5}$$

$\dot{m}$ refers to the fuel mass-flow and I_{sp} is the specific impulse, which is associated to a thruster characteristics. Moreover, spacecraft thrust acceleration is directly proportional to the thrust force, so that this term is also related to the fuel consumption.

$$A_{Thrust} = \frac{T}{m_{SC}} \tag{4.6}$$

Then, realizing that spacecraft mass is neglegible in the CRTBP, it arises that the best way to consider how optimal the fuel consumption of the mission has been is to minimize the spacecraft accelerations due to thrust usage. Therefore, the following objective function is put to work.

$$J = \int_{t_0}^{t_f} \mathbf{u}(t) dt \tag{4.7}$$

System governing equations

The system governing equations for the study case are the CRTBP ones, which are given by eq.2.20-25. However, those equations are not considering the control parameter. It only affects to the last three equations of the

CRTBP, which finally result in:

$$\dot{v_x} = 2v_y + x - \frac{(1-\mu)(x+\mu)}{r_1^3} - \frac{\mu(x-1+\mu)}{r_2^3} + a_{Thrust,x} \tag{4.8}$$

$$\dot{v_y} = -2v_x + y - \frac{(1-\mu)y}{r_1^3} - \frac{\mu y}{r_2^3} + a_{Thrust,y} \tag{4.9}$$

$$\dot{v_z} = -\frac{(1-\mu)z}{r_1^3} - \frac{\mu z}{r_2^3} + a_{Thrust,z} \tag{4.10}$$

The path constraints

Among all the variables compounding the Rendezvous problem, the ones related to the spacecraft control must limit their achievable values, indeed its path constraints. Control variables are modelling the spacecraft thruster performance, thus they must be constrained according the thruster technological limitations to represent reality as precise as possible. The thruster model has been defined using representative electric propulsion thruster values [22].

$$I_{sp} = 3000\ s \qquad\qquad T_{max} = 700\ mN$$

Control variables are representing accelerations. The thruster maximum acceleration can be calculated from the maximum thrust T_{max} attainable by the thruster using eq.4.6.

$$A_{Thrust,max} = \frac{T_{max}}{m_{SC}} \tag{4.11}$$

Spacecraft mass is known to vary along the space mission due to fuel consumption. Then, in order to be conservative in the analysis done, a large spacecraft mass value has been chosen. In this way, calculations are using the minimum maximum thrust that the spacecraft can generate along the whole mission. Moreover, it must be pointed out that only only one thruster is considered to be used during the mission, thus it can be ensured that the control variable results values calculated can be certainly attained by current available technology. Finally, the thruster path constraint read as follows:

$$\sqrt{a_{Thrust,x}^2 + a_{Thrust,y}^2 + a_{Thrust,z}^2} \leq A_{Thrust,max} \tag{4.12}$$

Note that A_{max} value must be converted into non-dimensional units. It can be simply done by using the conversion factor between dimensional and non-dimensional units provided in Chapter 2. Regarding the time variable, it

must be stated that it can only take positive values.

$$t \geq 0 \tag{4.13}$$

There would be also constraints in the position vector variables of the state vector, since both the volumes occupied by the Earth and the Moon cannot be penetrated by the spacecraft. Nonetheless, since the mission is designed far from those bodies, modelling this condition is meaningless.

The terminal constraints

The terminal conditions of the study problem are the target end of the mission position and velocity of the spacecraft. For some of the case analysis, the specific time at which this target state vector must be achieved will also be added to the before terminal constraints.

4.3.2 The Collocation method

When numerically implementing the optimal control problem, differential equations cannot be solved by a computer, thus the system governing equations constraints cannot be directly implemented. So as to solve this problem, it has been taken use of a collocation method. [23][24] Collocation methods enforce the dynamic equations to be fulfilled through quadrature rules or interpolation. In these methods, time is discretized by defining a set of nodes. Then, a suitable interpolating polynomial is selected such that it passes through the state values and maintains the state derivatives at each node interval. With this aim, Gauss-lobbato method has been used for obtaining the piece-wise continuous polynomial that satisfies the original equations of motion at discrete points.

Various discretization schemes with different simplicity and accuracy has been used.

- The third degree Gauss-Lobatto scheme, with integration order four, is also known as the Hermite-Simpson method, yielding a quadratic polynomial interpolant. This simple scheme is able to provide solutions by the spent of low computation resources and time. Nevertheless, it has limited accuracy in comparison of the next collocation method.

- The seventh degree Gauss-Lobatto scheme, with integration order twelve. It is very similar to the previous one, but with the advantage of

providing higher accuracy level. This scheme is formed by two interior points and three defect points between each pair of nodal points.

Note that truncation errors are always present in the collocation methods. In fact, the level of accuracy provided by these two mentioned methods can be understood by analyzing their local truncation error. The local truncation represents the error in the approximate integration over a subinterval $[t_i, t_{i+1}]$, it means, between two nodes of the problem mesh. Consider p_m be the polynomial in time of order m approximating the equations of motions given by $f(t)$. Then, the local truncation error takes this form:

$$\epsilon = \int_{t_i}^{t_f} f(t)dt - \int_{t_i}^{t_f} p_m dt \tag{4.14}$$

Third degree Gauss-Lobatto scheme - Hermite-Simpson method

In the Hermite-Simpson collocation scheme, a collocation point is defined between every two nodes of the grid. In order to generate a more intuitive understanding of this method implementation, an illustration representing the Hermite-Simpson method is provided.

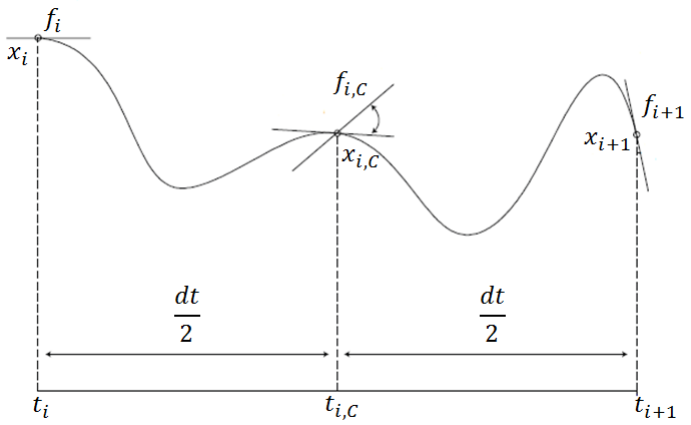

Figure 4.2: Hermite-Simpson method scheme representation.

The collocation point can be caluculated as follows:

$$\bar{x}_{i,c} = \frac{1}{2}\left(\bar{x}_i + \bar{x}_{i+1}\right) + \frac{\Delta t_i}{8}\left(\bar{f}_i - \bar{f}_{i+1}\right) \tag{4.15}$$

Although many optimal control solutions exists in the form of bang-bang solution, it is also necessary to ensure than an accurate historical of the control action along time is being performed by the provided collocation method to also allow constant thrust solutions. A trade-off between both competing control solutions is reached by the introduction of these collocation control points in the control state vector, thus increasing the reliability of the results of this collocation method. Then, the defect constraint minimizing the method error in the represented differential equations along the problem grid is given by the following equation.

$$|\Delta_{i,c}| = \bar{x}_i - \bar{x}_{i+1} + \frac{\Delta t_i}{6}\left(\bar{f}_i + 4\bar{f}_{i,c} + \bar{f}_{i+1}\right) \leq \epsilon \tag{4.16}$$

Seventh degree Gauss-Lobatto scheme

Larger number of defect points are considered between every node segment of the grid with the aim of increasing the order of the piece-wise polynomial used. Then, the internal points can be calculated as:

$$\begin{aligned}\bar{x}_{i,1} = {} & a_i^1\bar{x}_i + a_{i,2}^1\bar{x}_{i,2} + a_{i,3}^1\bar{x}_{i,3} + +a_{i+1}^1\bar{x}_{i+1}+ \\ & + \Delta t_i\left(v_i^1\bar{f}_i + v_{i,2}^1\bar{f}_{i,2} + v_{i,3}^1\bar{f}_{i,3} + v_{i+1}^1\bar{f}_{i+1}\right)\end{aligned} \tag{4.17}$$

$$\begin{aligned}\bar{x}_{i,c} = {} & a_i^c\bar{x}_i + a_{i,2}^c\bar{x}_{i,2} + a_{i,3}^c\bar{x}_{i,3} + +a_{i+1}^c\bar{x}_{i+1}+ \\ & + \Delta t_i\left(v_i^c\bar{f}_i + v_{i,2}^c\bar{f}_{i,2} + v_{i,3}^c\bar{f}_{i,3} + v_{i+1}^c\bar{f}_{i+1}\right)\end{aligned} \tag{4.18}$$

$$\begin{aligned}\bar{x}_{i,4} = {} & a_i^4\bar{x}_i + a_{i,2}^4\bar{x}_{i,2} + a_{i,3}^4\bar{x}_{i,3} + +a_{i+1}^4\bar{x}_{i+1}+ \\ & + \Delta t_i\left(v_i^4\bar{f}_i + v_{i,2}^4\bar{f}_{i,2} + v_{i,3}^4\bar{f}_{i,3} + v_{i+1}^4\bar{f}_{i+1}\right)\end{aligned} \tag{4.19}$$

As consequence of the increased number of internal points, three constraints must be satisfied at the nodes of the grid in order to ensure the fulfilment of the dynamic equation of motion. Despite the increase in complexity, a more accurate description of those motion equations are gained.

$$\begin{aligned}|\Delta_{i,1}| = {} & b_i^1\bar{x}_i + b_{i,2}^1\bar{x}_{i,2} + b_{i,3}^1\bar{x}_{i,3} + +b_{i+1}^1\bar{x}_{i+1}+ \\ & + \Delta t_i\left(w_i^1\bar{f}_i + w_{i,1}^1\bar{f}_{i,1} + w_{i,2}^1\bar{f}_{i,2} + w_{i,3}^1\bar{f}_{i,3} + w_{i+1}^1\bar{f}_{i+1}\right)\end{aligned} \tag{4.20}$$

$$\begin{aligned}|\Delta_{i,c}| = {} & b_i^c\bar{x}_i + b_{i,2}^c\bar{x}_{i,2} + b_{i,3}^c\bar{x}_{i,3} + +b_{i+1}^c\bar{x}_{i+1}+ \\ & + \Delta t_i\left(w_i^c\bar{f}_i + w_{i,2}^c\bar{f}_{i,2} + w_{i,c}^c\bar{f}_{i,c} + w_{i,3}^c\bar{f}_{i,3} + w_{i+1}^c\bar{f}_{i+1}\right)\end{aligned} \tag{4.21}$$

$$\begin{aligned}|\Delta_{i,4}| = {} & b_i^4\bar{x}_i + b_{i,2}^4\bar{x}_{i,2} + b_{i,3}^4\bar{x}_{i,3} + +b_{i+1}^4\bar{x}_{i+1}+ \\ & + \Delta t_i\left(w_i^4\bar{f}_i + w_{i,2}^4\bar{f}_{i,2} + w_{i,3}^4\bar{f}_{i,3} + w_{i,4}^4\bar{f}_{i,4} + w_{i+1}^4\bar{f}_{i+1}\right)\end{aligned} \tag{4.22}$$

A throughout explanation about this schmeme and the definition of the coefficient involved in eq.4.17-22 can be found in [25].

Finally, the Hermite-Simpsoon method has been selected for the study of the rendezvous problem, which it offered quite precise approximation of the CRTBP dynamics of motion at the cost of affordable computational time and memory resources.

4.3.3 IPOPT solver

IPOPT (**I**nterior **P**oint **Opt**imizer) is a software package that allows to solve smooth and twice differentiable nonlinear programs. In particular, it can be used for solving any kind of problem with the form:

$$min\ f(x) \qquad x \in \mathbb{R}^n \tag{4.23}$$

subject to

$$g^L \leq g(x) \leq g^U \tag{4.24}$$
$$x^L \leq x \leq x^U \tag{4.25}$$

where x are the optimization variables with possible lower and upper limits x^L ans x^U respectively and subject to the constraints given by $g(x)$; and $f:\ \mathbb{R}^n \to \mathbb{R}$ is the objective function. This solver is designed to find local solutions of mathematical optimization by using an implemented interior point line search filter method [26]. For a detail description about this solver and the mathematical algorithms involved, please refer to [27],[28].

4.3.4 Problem implementation

Introducing the objective function and the constraints into the non-linear programming solver implies writing those expression in a format which is understandable by the solver. OPTI Toolbox [27] interface has been used with that purpose. It is a matlab based tool developed for solving any type of optimization problem by using some non-linear programming solvers, as IPOPT. This interface requires expressing the optimization problem in the following way.

$$min_x \quad f(\mathbf{x}) \tag{4.26}$$

subject to

$$A\mathbf{x} \leq b \tag{4.27}$$
$$A_{eq}\mathbf{x} = b_{eq} \tag{4.28}$$
$$c_l \leq c(\mathbf{x}) \leq c_u \tag{4.29}$$
$$l_b \leq \mathbf{x} \leq u_b \tag{4.30}$$

f is the objective function, which has to be an scalar function; $\mathbf{x}$ is the vector to optimize; A and A_{eq} is a matrix containing the linear inequality and equality constraints; $c(\mathbf{x})$ represent the non-linear constraints; and l_b, u_b stands for the boundary values of the optimization vector. Note that equality non-linear constraints can be stated through taking $c_l = c_u$.

Referring to the problem which motivates this thesis, the optimization vector must be compounded by the following variables:

- X: It refers to the six degree of freedom state vector completely defining the spacecraft motion.

  $$X = [x, y, z, v_x, v_y, v_z]^T$$

  Please, recall that the problem has been time discretized to implement the collocation method. Therefore, each of the above values has 1 times the number of nodes of the grid size. Then, taking n as the total number of nodes discretizing the problem, this vector has dimensions $[1, 6n]$.

- X_c: According to the collocation method used, every dynamic variables must have its associated control point. Hence, X_c is a vector with dimensions $[1, 6n]$.

- F: This vector contains the control variables associated to each node.

  $$F = [a_x, a_y, a_z]^T$$

  In contrast to the vector of the state vector, it has dimensions $[1, 3n]$, since the control variables are half the state vector ones.

- F_c: In this vector it is stored the collocation points associated to the control variables. It has the same dimensions than F.

- t: It defines the grid distribution used in the problem, thus has a dimensions the number of nodes involved ($[1, n]$).

- t_f: Unique variable stating the time at which the terminal constraints must be fulfilled.
- dt: Unique variable defining the separation between the grid nodes. It is one-dimensional since the grid has been distributed uniformly.

The optimized vector used for solving the problem is obtained by grouping all these variables into a single vector. Using the Hermite-Simpson method, it has dimensions $[1, 17n + 2]$.

$$\mathbf{x} = [X, X_c, F, F_c, t, t_f, dt]^T \tag{4.31}$$

The objective function

The formula of the objective function derived in section 4.3.1 (eq.4.7) must be implemented. Using the notation related to the numerical implementation, that integral will result in this equation.

$$f(\mathbf{x}) = \sum_{i=1}^{n} \sqrt{a_{x,i}^2 + a_{y,i}^2 + a_{z,i}^2} \cdot dt \tag{4.32}$$

Linear Constraints

The linear constraint of the problems are the ones concerning the initial and final conditions and the time grid. The former can be easily implemented by writing this equality condition in the form given in eq.4.28-29. The initial conditions have been introduced as an equality constraint whilst the final ones have been implemented as a inequality constraint in order to allow some tolerance. Regarding the time relations, firstly it must be defined the temporal grid distribution.

The grid has been uniformly distributed by taking the variable dt as a constant through the calculations (although it must be noticed that its value is not fixed for the solver unless it is specified). Thus, the time relations between the temporal variables are given by:

$$t_i = t_0 + i \cdot dt \tag{4.33}$$

where t_i refers to each of the n variables defining the grid of the problem. Then, consistency with the final temporal value must be assessed, which it is done by implementing the following constraint.

$$dt - \frac{tf}{n-1} = \frac{t_0}{n-1} \tag{4.34}$$

For some of the study study cases, specify the final time at which the final position has to be reached is a must. For such cases, neither t_f or dt (since they are coupled) must be modified by the solver, so that an additional equality constraint has been added for taking into account this fact. This constraint would add an additional row and column to the matrix A_{eq} of eq.4.28.

Non-linear Constraints

Two different non-linear constraints are involved in the problem: the equations concerning the collocation method and the thrust model. Eq.4.15-16 must be implemented for describing the equations of motion of the problem, which would results in $6(n-1)$ constraints. In regard to the thrust model, eq.4.12 must be used, implying $9n$ additional non-linear constraints.

Solution Initial guess

IPOPT solver, as any non-linear optimazation program, requires of an initial condition of the optimization vector from which iterate up to converge in the optimal solution. Providing a consistent initial guess uses to be crucial for the solver to converge in an optimal solution. Otherwise, the program might return that the problem is infeasibly when actually the initial condition is too far from the solution. Hence, it has been provided as initial guess the natural Halo trajectory without any thrust manoeuvres. In this way, it is provided a conditions which is already fulfilling the constraints related to the governing equations of motion of the problem.

Program tolerances

When numerically implementing this problem, tolerance must be defined for considering the some constraints are being fulfilled. For the non-linear constraints implementing the collocation method, it has been allowed an error of the order 10^{-10}. Thus,

$$c_l = -10^{-10}, \qquad c_u = 10^{-10}$$

Regarding the final conditions, also a tolerance of 10^{-10} has been considered. It means, it has been considered that the problem has reached the target final state conditions when:

$$|\vec{x}_{Solution}(tf) - \vec{x}_{target}(tf)| \leq 10^{-10}$$

This implies that the allowed error for the spacecraft rendezvous will be in the order of centimetres when expressing it into dimensional units, which can be considered negligible for the problem on purpose.

4.4 Discussion of Results

In Section 4.2, a detail description about the cases of study has been provided. Hereafter, the results associated to those are going to be presented. In addition, an exhaustive analysis of those results is performed. ΔV parameter, which is the total acceleration that the thruster must provide during the mission, and thus is directly related to the propellant consumption and indeed cost of the mission; and the transfer time are the main variables from which extract information about the trajectory performance. Please, note that with sake of generality, the results are provided in non-dimensional units.

4.4.1 Case 1 - Halo Manifold Insertion

It must be reminded that the objective of this first case is analyze the spacecraft insertion in an halo manifold so as to travel to an transition halo different to the one where rendezvous is targeted. In the following figure, it can be appreciated the kind of manifold trajectory that the spacecraft must follow so as to reach the target position at the minimum cost of propellant possible.

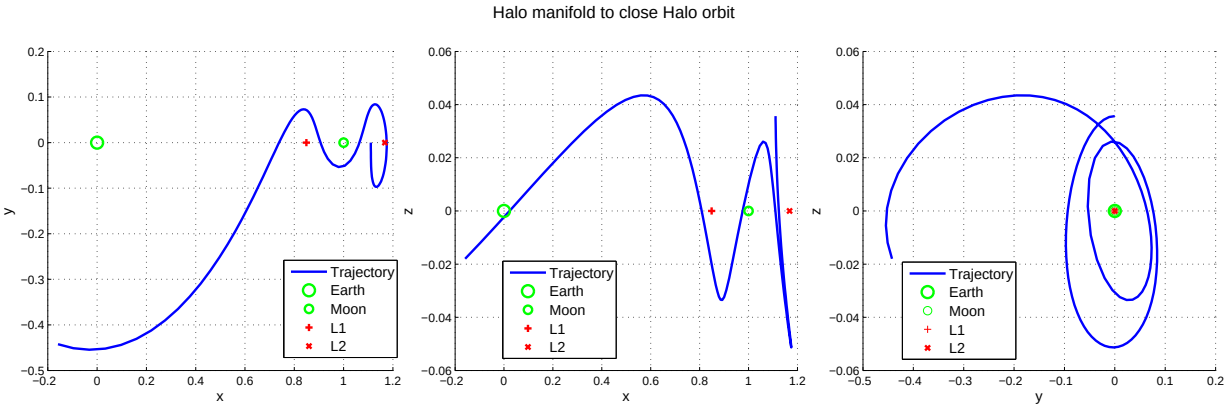

Figure 4.3: Optimal trajectory for the spacecraft injection in the transition L_2 Halo orbit.

Analyzing the thrust usage needed for performing this mission (Figure 4.4), it must be pointed out several aspects. Firstly, it is noticed that

although the spacecraft seems to be following a manifold, some corrections seems to be needed to perform by the thruster. The difference existing between the integration scheme using in the initial manifold calculation (which have been used for calculating the departure point), in fact *ode45* matlab integrator; and the one provided in the control problem optimization, Hermite-Simpson integration scheme, could lead to the necessity of a small part of this correction. Nonetheless, the greatest part of the correction are expected due to the fact that the arrival orbit is not the target one. Then, as the manifold departure position has been calculated for the target orbit, some correction are obviously required by the thruster in order to adjust its trajectory for arriving the planned position in this case. Please, recall that the definition of this particular case was motivated by the aim of analyzing how small errors (which could result at any mission for any reason as external factors or technological accuracy limitations) in the initial condition of the halo or in the selection of the arrival orbit can impact the mission fuel cost.

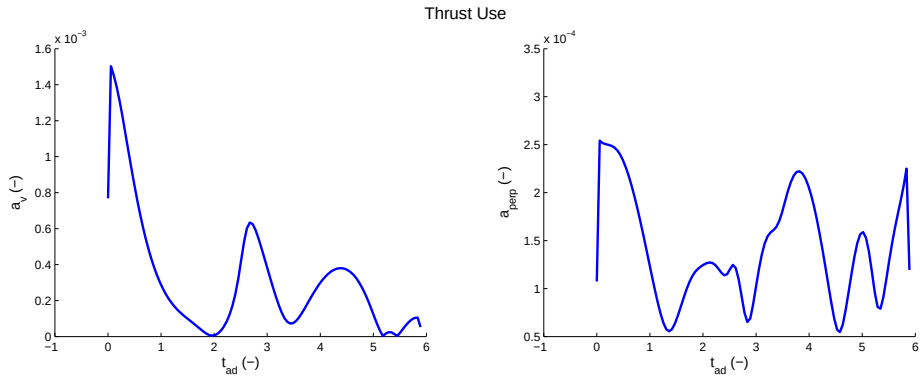

Figure 4.4: Optimal thrust control actuation during the Halo manifold injection manoeuvre.

Secondly, it is observed that the main thrust correction must be done in the direction of displacement of the vehicle, since one order of magnitude of difference is found between the tangential accelerations and the ones perpendicular to those. Notice that in Figure 4.4, the graph on the left shows the magnitude of the thrust acceleration performed along the velocity direction whilst the graph on the right shows the perpendicular ones. Lastly, analyzing the time that has been needed to follow the optimal trajectory, an estimation about transfer time for travelling to an L_2 is obtained. From this

mission, it is deduced that this transfer uses to require about 26 days and 14 hours, which is the time corresponding to 6 non-dimensional time units.

Parametric Analysis

A parametric analysis varying the initial position departure position by a small drift, it is studied the effect on delaying or anticipating the departure start respect to the target one. This results are depicted in Figure4.5.

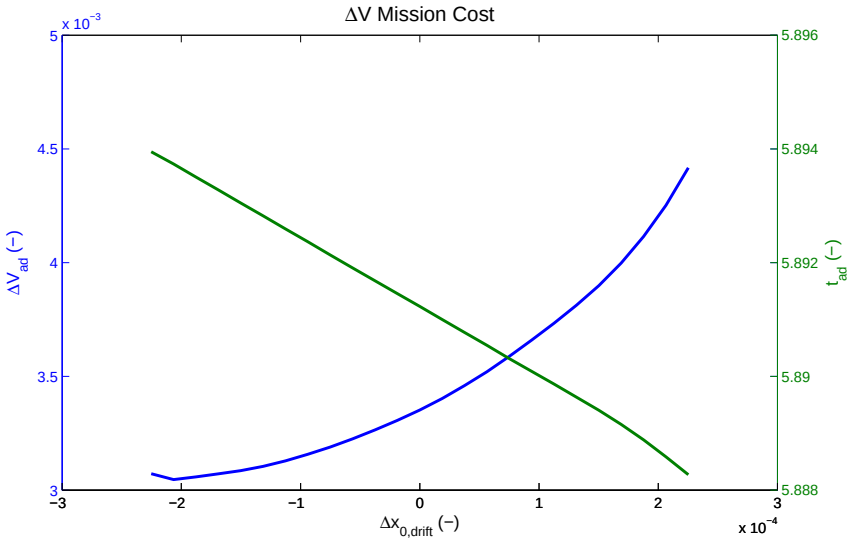

Figure 4.5: ΔV Mission cost depending on the initial departure point.

It can be appreciated that for positive drift displacements from the initial departure position, the ΔV cost of the mission increases, thus more propellant is consumed. This result seems to be coherent with expectations since as the departure position gets away from the optimal one, the mission cost should increase. In addition, it is also consistent the fact that slightly lower time is required for those new missions, since a positive drift displacement implies departing a bit closer from the Moon, so that shorter transfer times were expected.

Regarding the negative drift displacement results, they seem to be surprising in first approach. Nonetheless, it must be recalled once again that the departure orbit has not been calculated for the target Halo destination of this case analysis, instead it is calculated for the final targeted Halo orbit. Thus, it seems that the optimal departure position for the Halo orbit of destination in this case is located at a negative drift position respect to

the one currently used. On the other hand, transfer time continues being consistent to the previous analysis, since as negative drift positions are further form the Moon and hence from the L_2 point, more time is required in the mission.

4.4.2 Case 2 - Transfer between Halo orbits

The solution to this optimization problem can be seen in the following graph. The initial guess (I.guess) line corresponds to the initial trajectory that it has been introduced to the optimization solver; the solution line shows the final optimized trajectory and the initial and final position indicators show the departure point of the mission, which is associated to the point of the halo orbit reached in case 1, and the arrival point of the mission respectively, which belongs to the halo orbit in which rendezvous is pretended.

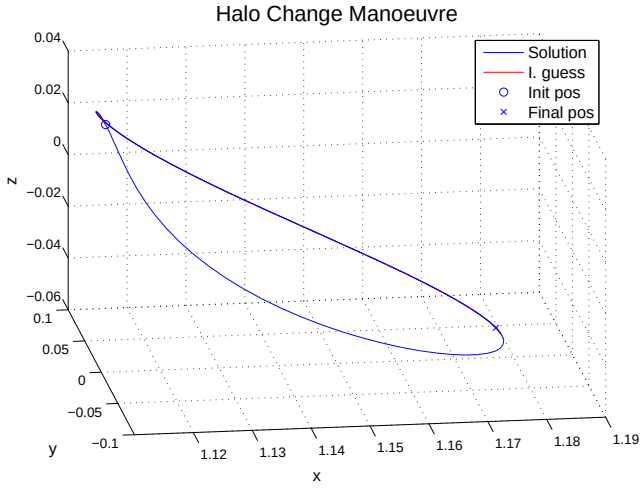

Figure 4.6: Optimal trajectory for the Halo orbit transfer.

It also can be clearly appreciated that the optimal trajectory for reaching the new Halo consists on making a complete orbit with small thrust corrections before trying to inject the spacecraft to the new orbit. This result seems to be logical since the arrival Halo has greater amplitude than the departure one. Therefore, the spacecraft takes advantage of the slightly unstable nature of the departure Halo in order to increases its amplitude and becomes closer to the arrival one, in such a way that the spacecraft manoeuvres are reduced to the minimum. This solution have been obtained

since no time constrictions have been considered.

Analyzing the thruster behavior, it can be observed that in the mission tangent acceleration are combinated with perpendicular ones, as opposed to the previous case. Moreover, the order of magnitude of this case is some orders of magnitude lower than the previous case. It turns out then than changing from Halo orbit seems to not be very costly in terms on fuel. Therefore, a mission design strategy for this case about looking for the halo manifold whose injection from Earth is more favourable might be prioritize respect to choosing the one corresponding to the target orbit, since the cost of halo orbit changes seems to be negligible in comparison to the one faced in the from Earth halo orbit injection.

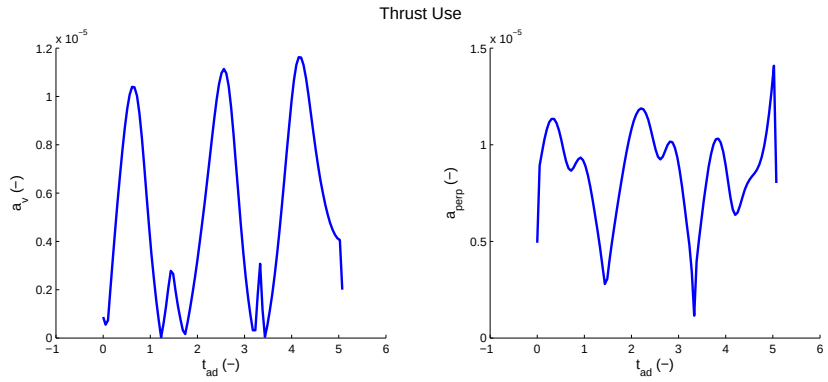

Figure 4.7: Thrust Control optimal solution for the Halo orbit transfer.

The Mission Fuel Cost versus the required Transfer Time

A study between different initial departure Halo position and different arrival Halo position can lead to an analysis of transfer time vs optimal ΔV budget trade-off for these studied Halos. Then, rendezvous mission would be a synchronization problem.

An schematic of the departure points is provided in Figure 4.8. The same distribution of points has been taken for the target halo, so this schematic is also going to be used for providing the information about the arrival points (although it must be recalled that they belong to an orbit with 50 km of amplitude more than the one shown in the graph). In the following graphs, the number expressing the departure and arrival position will indicate the position at which they are in the orbit.

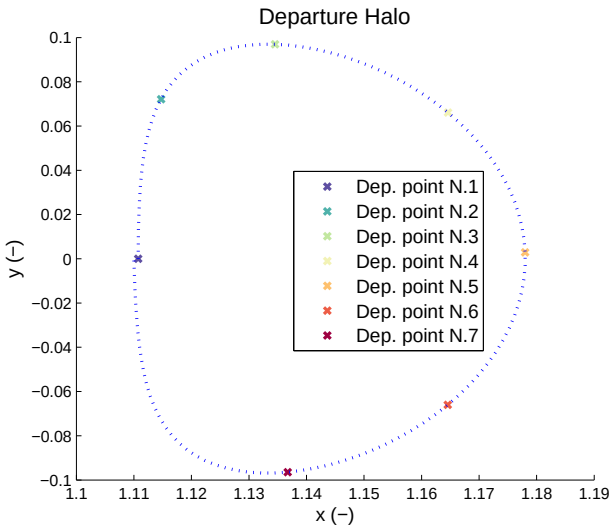

Figure 4.8: Departure Halo orbit points.

The results for this case analysis are grouped in Figure 4.9 and Table 4.1. In the figure, the associated optimal ΔV for every departure-arrival mission profile is shown. x-axis accounts for the different arrival positions that have been investigated (recall that it corresponds with points shown in Figure 4.8, but with the difference that in the orbit where they are set is greater in amplitude). Then, different lines are drawn showing the results for departing at every of the points shown in Figure 4.8.

For starting the analysis of this case, the information in Table 4.1 must also be considered, since it shows the transfer time information associated at each pair of departure-arrival points.

From this analysis, the optimal transfer solutions for the given problem is obtained.

- The best case in terms of ΔV is the mission departing at position 1 and arriving to the point 5 of the target orbit. It will cost $\Delta V = 6.594 \cdot 10^{-2}\ m/s$. It must be noticed that this value is similar to the one needed for station keeping in a general L_2 Halo orbit. A similar manoeuvre is being performed in this case, so this result seems to be consistent.

- In terms of time, mission from departure point 1 to the arrival point 2 provides the best solution. $t_{ad} = 0.41134 \rightarrow t = 42.92\ h$

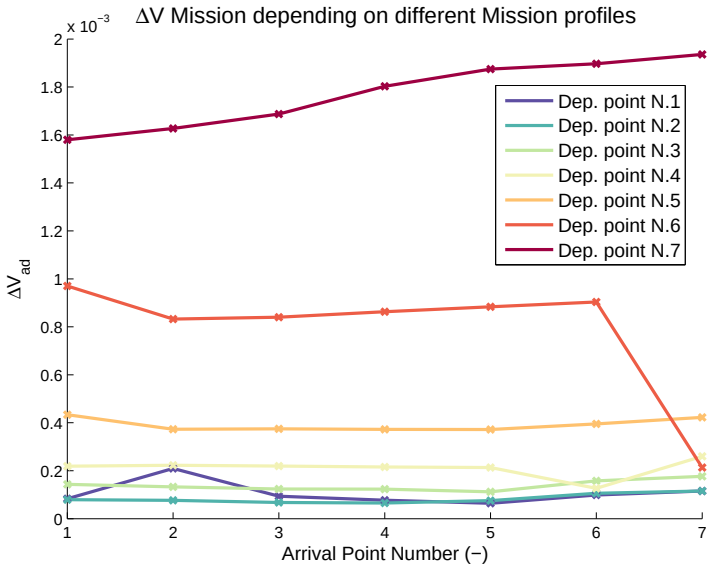

Figure 4.9: Mission ΔV depending on the mission profile definition.

		Arrival point						
		#1	**#2**	**#3**	**#4**	**#5**	**#6**	**#7**
Departure Point	**#1**	3.3935	0.4113	0.8227	1.2683	1.6796	2.1252	2.5365
	#2	2.9821	3.3935	3.8048	4.2504	1.2683	5.1074	2.1252
	#3	5.9643	2.9821	3.3935	3.8391	0.8570	4.6960	5.1073
	#4	2.1252	2.5365	2.9479	3.3935	3.8048	0.8569	4.6617
	#5	5.1071	2.1250	2.5364	2.9820	3.3933	3.8389	4.2502
	#6	4.6608	1.6787	2.0902	2.5358	2.9470	3.3926	0.4113
	#7	0.8548	1.2661	1.6776	2.1233	2.5345	2.9799	3.3912

Table 4.1: Transfer times (given in adimensional units) of the different Mission profiles defined in Figure 4.9. As reference, 3 units nondimensional time corresponds to 3 days and 1.08 hours.

Although propellant cost uses to drive the mission selection, be aware of

the minimum time at which the spacecraft can perform the mission can be highly important in emergency situations.

Nonetheless, for selecting the proper mission for a particular space mission, a trade-off study between the ΔV cost and the transfer time must be investigated. The obtained ΔV values depend on several factors. As long as the transfer increase in a significant way, the ΔV starts also to growth. Although in these long manoeuvres the thrust ΔVs are low, the fact that the thruster must be used for long time is responsible of the huge ΔV increase. On the other hand, finding stable manifolds along the optimized solution search by the solver allow to greatly reduced the ΔV of the mission. On the contrary, if the vehicle has to travel through the unstable region of the Halo, more correction manoeuvres will be needed to perform. In fact, this last effect seems to cause the larger ΔV cost found when departing from the points 6 or 7 of the Halo orbit.

It must be also pointed out that information about the trajectory spatial shape is also provided by the graph and the table. Knowing that the departure halo orbit period is around 3.35 in adimentional units, it can be deduced if the optimal arrival point is attained by direct injection, for cases where the transfer time is lower than that value; or by slowly escaping from the departure halo orbit taking advantage of its unstable nature.

Lastly, it has to be noticed that in the table diagonal the time values are very close. It results from the fact that the at those cases the spacecraft has to travel to the same point number but in a different orbit. Thus, the transfer time last around the time period of the orbit, as expected, with slightly differences due to the different trajectories followed for reaching its calculation.

4.4.3 Case 3 - Rendezvous in the target Halo orbit

This problem aims to reach some halo orbit position belonging to that halo orbit in a different time that it occurs naturally, it means, it is wanted to accelerate or decelerate the spacecraft along the Halo orbit. An illustrative example of this process comes from the case of considering a target and a chaser spacecraft in the same Halo orbit. Then, in order to get that the chaser meets the target, it has to accelerate or decelerate along the Halo orbit to rendezvous. Recall that for this problem, the following Halo orbit has been used.

- L_2 Halo orbit with amplitude of 95000 km.

- The spacecraft need to reach half of the orbit one hour before it would occur without using any propellant. (This time is equivalent to 0.0095 adimensional time units).

In the following graph, it can be observed how the spacecraft follows the Halo orbit with small differences but reaching exactly the final position. *Sol* corresponds to the optimal trajectory and the *I.Guess* is the natural Halo orbit trajectory. In this way, the spacecraft is able to reach the destination place at the specified time.

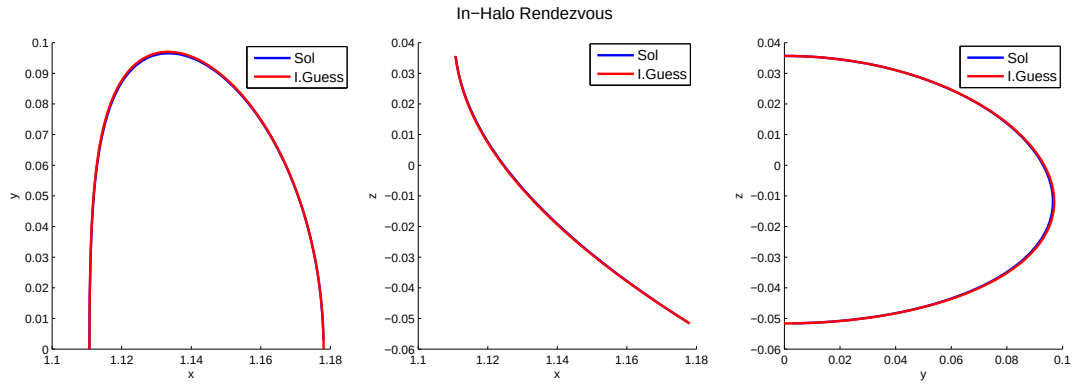

Figure 4.10: In-halo rendezvous optimal trajectory.

Lastly, the control law that the spacecraft must use for following the desired trajectory is depicted next. It can be observed that it satisfies the technology capability limit specified for the spacecraft propulsion system. The maximum acceleration that the thruster can provide is $2.57 \cdot 10^{-3}$ non-dimensional acceleration units.

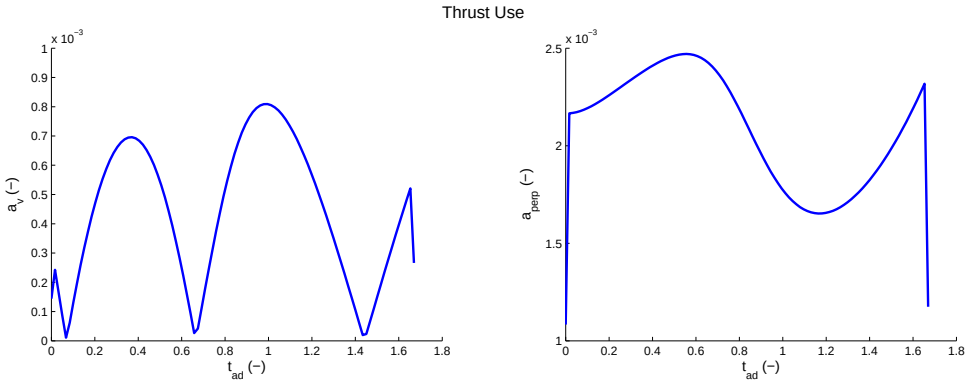

Figure 4.11: Optimal Thrust actuation for the in-halo rendezvous.

Parametric Analysis

For this problem, different target times to reach the final position (with stands for different rendezvous cases) can be analysed in order to try to identify some preferred manoeuvre which would be useful to prioritize in order to be able to rendezvous at the minimum cost of fuel possible. The results are gathered in the next figure.

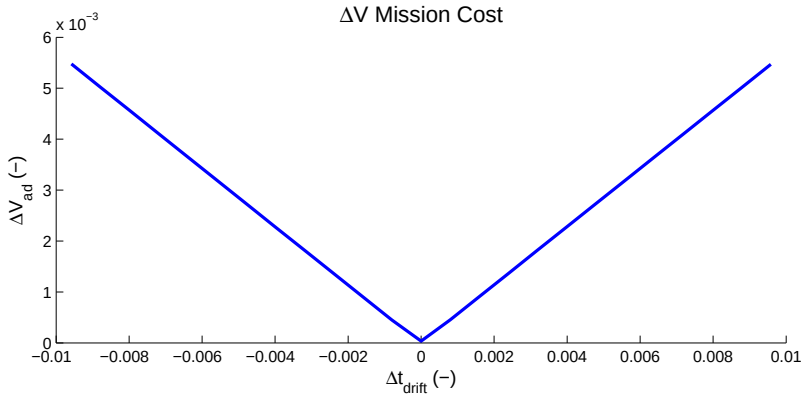

Figure 4.12: ΔV Mission cost depending on the out-of-phase time between the chaser and the target.

The time separation between target and chaser phases presented in non-dimensional units corresponds to real separation times of -1h to 1h in the

Earth-Moon system. The result observed seems to be coherent with what was expected. Moving at the halo orbit at the natural orbit speed yields in a zero fuel cost mission. Then, as long as accelerating or decelerating along the orbit is pretended, the mission cost increases since thrust actuators must be used. Also, it must be pointed out that for this small time differences, the ΔV cost associated for these rendezvous missions seems to be linearly related with the time separation between spacecraft.

Lastly, it must be noticed that since slowing down or accelerating manoeuvre for the chaser to rendezvous the target is equivalent in terms of ΔV, it is supposed that the same thruster usage must be done but with opposite directions. This result can be clearly appreciated in Figure 4.13. This time, accelerations are given in a rotating reference frame used along all the project, so that x-acceleration goes in the Earth to Moon direction, y-direction is perpendicular to it but contained in the Earth-Moon rotating plane, and z-direction orthogonal to the before ones; since this frame offers a clear perception of how these accelerations are totally opposed so that the solutions are symmetric.

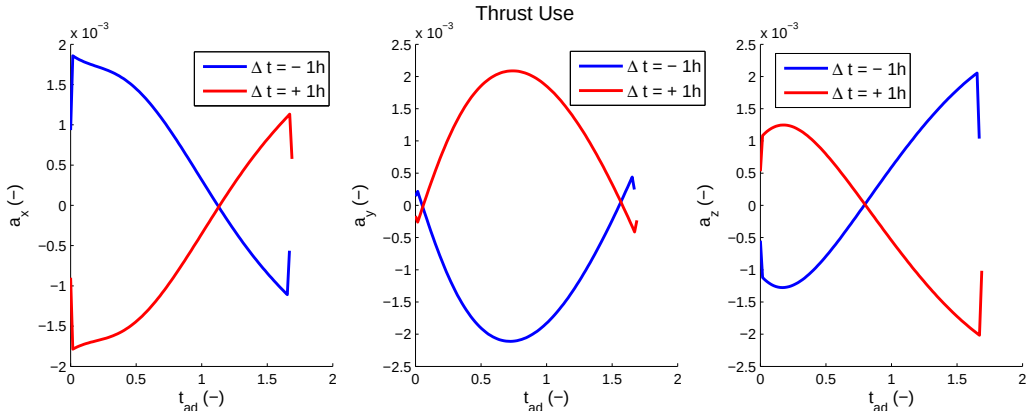

Figure 4.13: Thruster actuation for two mission with opposite Δt_{drift} in sign.

4.4.4 Rendezvous Problem Results

With means of completeness, an additional general rendezvous problem covering the three before cases has been defined. Although subdividing the problem in several subcases has allowed to investigate different challenges

present in a rendezvous mission as well as all the possibilities that could arise when targeting a rendezvous mission in a non-Keplerian orbit such as the L_2 halo orbit, treating a problem as a unique mission is interesting to be studied. Furthermore, all the previous analysis has been used for properly define this mission.

Then, the initial departure position from the Earth has been kept. Then, for the selection of the arrival point in the final target orbit, Case 2 results have been considered. According to Figure 4.9, the final position with lowest expected ΔV correspond to the arrival point N.5 (see Figure 4.8), so that position has been defined as the target final position of the mission. The calculated optimal trajectory for such mission is depicted hereafter. During the mission, the spacecraft seems to follow also a manifold trajectory and then it slowly gets injected in the desired Halo orbit.

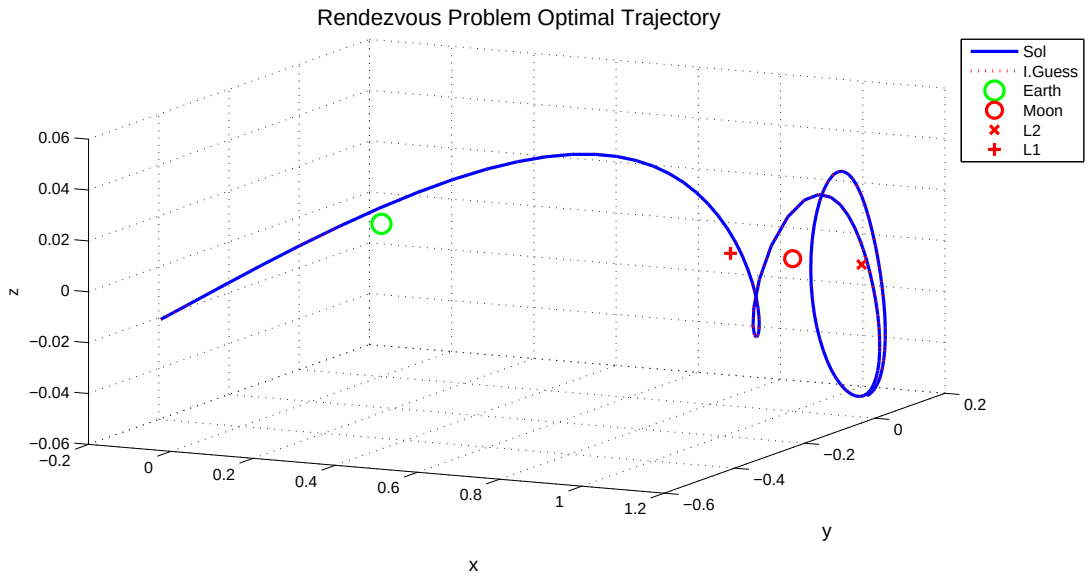

Figure 4.14: Optimal trajectory design for the Rendezvous Problem.

Comparison with complete result using the submission cases

Study the effect from making the trajectory optimization in one step or subdiving it in several stages must be analyzed. Regarding the vehicle trajectory, it can be observed that in both cases the spacecraft follows almost the same path.

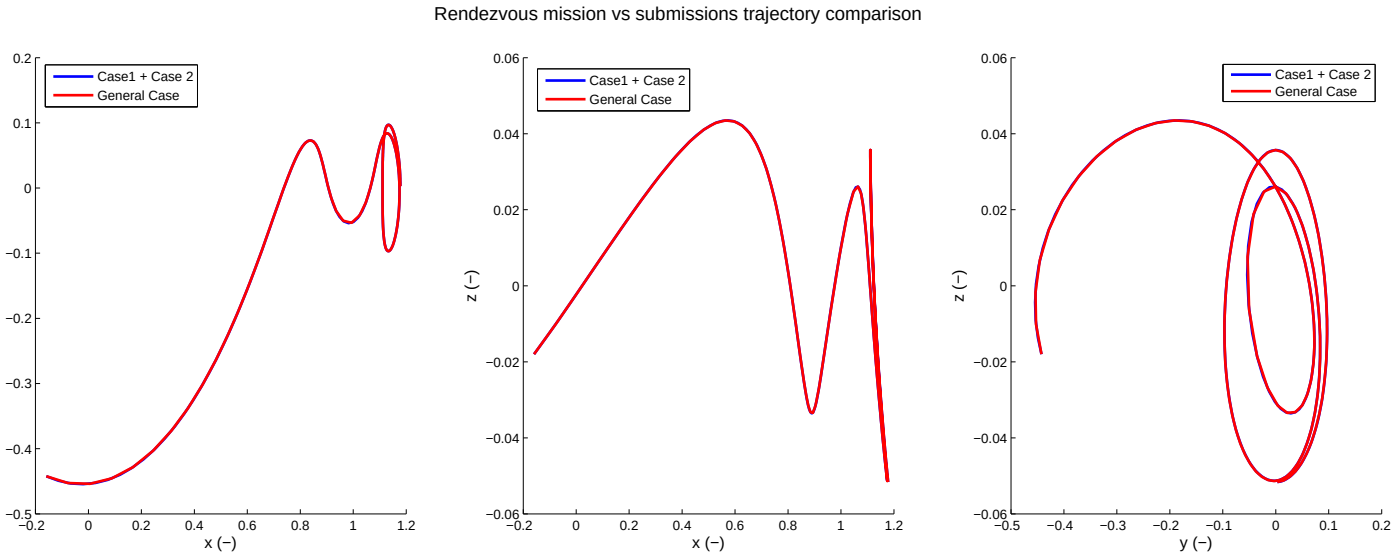

Figure 4.15: Trajectory comparison between global rendezvous versus rendezvous by executing the submissions.

Comparing the thrust accelerations profile, larger differences are encountered. The thrust acceleration direction are similar, which explains that both cases follows a very close trajectory. Nonetheless, a great difference is appreciated around non-dimensional time equal to 6. It is totally consistent with what is expected, since around that time the case grouping the subcases 1 and 2 the spacecraft is injecting into the transition L_2 halo orbit. On the contrary, directly targeting the final orbit position avoid that huge waste in propellant consumption. Regarding the transfer time involved, it cannot be appreciated any significant difference, as it can be observed in Figure 4.16.

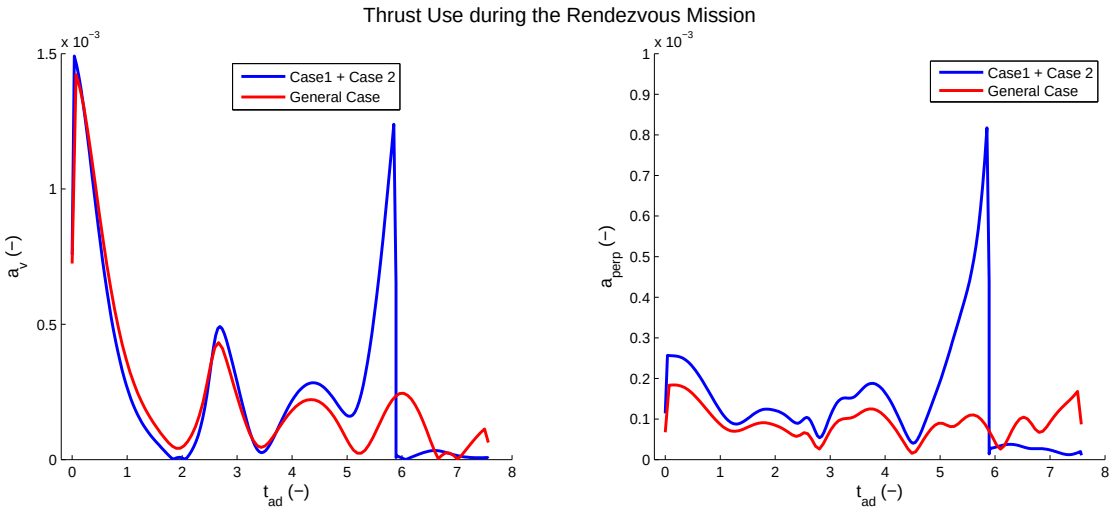

Figure 4.16: Thrust Control activation during the manoeuvre.

4.5 Conclusions

A detailed analysis of the different rendezvous missions which can be target at a L_2 halo orbit has been done. It has been found that the most demanding parts in term of propellant cost (or equivalently ΔV cost) are the insertion from the Earth parking orbit and the rendezvous mission when both spacecraft are set in the same halo orbit. Thus, it has been shown that synchronizing the rendezvous mission is preferred in order to avoid a large final correction along the same halo.

Chapter 5

Conclusions and Future Work

This chapter is divided in two parts. Firstly, the conclusions that have been obtained from realizing this master thesis are presented. Then, it is analyzed the future work that can be done from the current state of the art gained with this project.

5.1 Conclusions

In this thesis, it has been thoroughly studied the designed process that any space engineer must follow for determining the appropriate trajectory for reaching a space destination. This process commences with the definition of the mission target requirements. Once they are clearly stated, a general study about the orbits which are expected to fulfil those requirement is performed, selecting the best candidates from a comparative analysis. Then, a detail investigation of the chosen orbits must be done. It involves both the creation of a numerical model which allows to have a trustworthy representation of the real behaviour of those and the study of their dynamical characteristics. Afterwards, an extensive study of the possible trajectories meeting the required objectives must be realized. Once a suitable trajectories has been investigated, they have to be optimized in order to consume the less resources possible for reaching the objective. Lastly, a detail analysis of these results must be done in order to asses whether further analysis is needed or an optimum trajectory has been obtained.

In particular, the trajectory design process of this thesis has been focused in the Earth-Moon system. Space exploration needs have been identified in this system. Some slightly explored non-keplerian trajectories have been found to greatly adjust to cover those needs. Investigating those trajectories, it has been noted that, concretely, L_1 and L_2 halo orbits and NROs greatly satisfies the upcoming exploration needs.

Once it have been noticed the orbits at which an spacecraft is intended to travel, the trajectory design process begin. A numerical model of the Earth-Moon system has been generated in order to simulate the environment in which the spacecraft will move. Then, L_1 and L_2 halo orbits and NROs have been found and their dynamical properties have been simulated. The existence of free-consumption trajectories called manifols departing and arriving to those orbits have been noticed, so how reaching those trajectories have been analyzed.

A space mission has been defined afterwards. Rendezvous in a L_2 Halo orbit from a spacecraft travelling from an Earth orbit has been targeted. In this way, the procedures for designing any kind of space mission, and in particular subjected to the constraints faced in the Earth-Moon system, has been carried out. All the possible cases for making rendezvous at the target L_2 has been analyzed: rendezvous from an Earth parking orbit, rendezvous from a close halo orbit and catching the target spacecraft when it is departed at the same halo but at a distinct position in the orbit.

All the cases have shown to be feasible for being performed with the use of EP (Electric Propulsion) thruster. The final optimal trajectories for those cases are presented in this thesis. In addition, it has been shown than exploding the stability properties of the orbits involved in the problem allows to greatly reduced the mission cost in terms of fuel consumption (or ΔV).

Thus, after completing this thesis, it can be considered that the intended project goals have been successfully met. In fact, all the processes involving an optimal trajectory design for an intended mission have been studied in detail.

5.2 Future work

Similar analysis to the one performed with the rendezvous mission in the L_2 has been tried out for the NRO at the last stages of this thesis development, since it is the other orbit of interest for future space missions. A first trajectory trial has been done by using the results from the rendezvous L_2

halo mission. The unstable manifolds of the L_2 orbit has been analyzed in order to try reaching a trajectory joining these manifolds with the stable ones of the NRO. Then, this trajectory could be optimized using the CRTBP optimizer developed during this thesis.

Unfortunately, the first optimization analysis consisting in reaching the NRO orbit from the L_2 Halo referred along this thesis did not converged. Due to lack of time, this analysis have been left for future analysis. Nonetheless, the basis allowing calculating this trajectory is already done, since same processes and optimization models that the ones used during the rendezvous mission in the L_2 halo orbit are needed. In fact, since the NRO dynamics is fully studied, the remaining step is searching for only one orbit in the L_2 halo family whose unstable manifolds gets close to the target NRO. Up to now, this process has only been carried out for one L_2 halo orbit. Then, after improving the initial trajectory guess and testing many possibilities, the developed optimizer is expected to find an optimal solution.

Other branches of investigation can be also followed from this project.

1. Increase the accuracy of the models used for describing the Earth-Moon system. For instance, disturbance forces can be added to the existing model or even, the effect of the eccentricity of the Moon orbit around Earth can be modelled .

2. Widen the rendezvous mission to other non-keplerian trajectories existing in the Earth-Moon system. For instance, there are near rectilinear trajectories joining some L_1 and L_2 halo orbits. Analyzing how costly would be rendezvous might help for investigating whether exists better unexplored places for making the rendezvous manoeuvre.

3. To realize the same rendezvous study in other system fulfilling the CRTBP conditions so as to analyze of how different the relation between the two massive bodies affect the mission results.

Bibliography

[1] A. McInnes, *An Introduction To Libration Point Orbits.* 2009.

[2] R. Whitley and R. Martinez, "Options for staging orbits in cis-lunar space," 2015.

[3] W. Pratt, C. Buxton, S. Hall, J. Hopkins, and A. Scott, "Trajectory design considerations for human missions to explore the lunar farside from the earth-moon lagrange point em-l2," 2013.

[4] J. Marsden and T. Ratiu, *Introduction to Mechanics and Symmetry, volume 17 of Texts in Applied Mathematics.* Springer-Verlag, 1999.

[5] J. M. James, *Celestial Mechanics Notes Set 4: The Circular Restricted Three Body Problem.* 2006.

[6] H. Schaub and J. Junkins, *Analytical Mechanics of Space Systems, Third Edition.* AIAA Education Series, 2014.

[7] R. H. Battin, *An Introduction to the Mathematics and Methods of Astrodynamics, Revised Edition.* AIAA Education Series, 1999.

[8] A. K. Pal and B. S. Kushvah, "Geometry of halo and lissajous orbits in the circular restricted three-body problem with drag forces," 2014.

[9] D. L. Richardson, *Analytic construction of periodic orbits about the collinear points.* Celestial Mechanics, vol. 22, p. 241-253, Oct. 1980.

[10] W. Koon, M. Lo, J. Marsden, and S. Ross, *Dynamical Systems, the Three-Body Problem and Space Mission Design.* 2004.

[11] G. Gómez, J. Llibre, R. Martínez, and C. Simó, *Dynamics and Mission Design Near Libration Points, Vol. I Fundamentals: The Case of Collinear Libration Points.* World Scientific, 1980.

[12] K. C. Howell, *Three-Dimensional Periodic Halo Orbits.* Celestial Mechanics, Vol. 32, Issue 1, p. 53, 1984.

[13] H. Vermeiden, "Optimal translunar lagrange point orbits for olfar," Master's thesis, Delft University of Technology, 2014.

[14] R. Tiwary, D.-V. Srivastava, and B. Kushvah, "Computation of three-dimensional periodic orbits in the sun-earth system," 2018.

[15] G. P. Alonso, "The design of system-to-system transfer arcs using invariant manifolds in the multi-body problem," Master's thesis, Purdue University, 2006.

[16] D. Gordon, "Transfers to earth-moon l2 halo orbits using lunar proximity and ivariant manifold," Master's thesis, Purdue University, 2008.

[17] T. V. Escribano, "Poincaré sections and resonant orbits in the restricted three-body problem," Master's thesis, Purdue University, 2010.

[18] C. Ponssard, K. Graichen, N. Petit, and J. Laurent-Varin, "Ascent optimization for a heavy space launcher," 2009.

[19] R. Serban, W. Koon, M. Lo, J. Marsden, L. Petzold, S. Ross, and R. Wilson, "Halo orbit mission correction maneuvers using optimal control," 2000.

[20] T. . N. Y. . . Robert E. Pritchet, School = Purdue University Master's thesis.

[21] B. A. Conway, *Spacecraft Trajectory Optimization.* Cambridge University Press, 2010, 2010.

[22] D. Grebow, M. Ozimek, and K. Howell, "Design of optimal low-thrust lunar pole-sitter missions," 2011.

[23] J. F. Herman, "Improved collocation methods to optimize low-thrust, low-energy transfers in the earth-moon system," Master's thesis, University of Colorado at Boulder, 2015.

[24] D. Grebow, M. Ozimek, and K. Howell., "Design of optimal low-thrust lunar pole-sitter missions," 2009.

[25] M. Ozimek, D. Grebow, and K. Howell, "A collocation approach for computing solar sail lunar pole-sitter orbits,"

[26] D. M. González, "A comparative study of optimal control algorithms using ideal frame references," Master's thesis, Universidad Politécnica de Madrid, 2014.

[27] A. S. Vigerske, *Introduction to Ipopt: A tutorial for downloading, installing, and using Ipopt.* Technical report, Carnegie Mellon University, 2014.

[28] A. Wächter, "An interior point algorithm for large-scale nonlinear optimization with applications in process engineering.," Master's thesis, PhD thesis, Carnegie Mellon University, Pittsburgh, 2002.

Appendix A

Results: Complementary material

Some additional complementary graphical information regarding the results of this thesis is gathered in this appendix. They might help to better understand the results at which they are referred.

A.1 General Rendezvous Problem

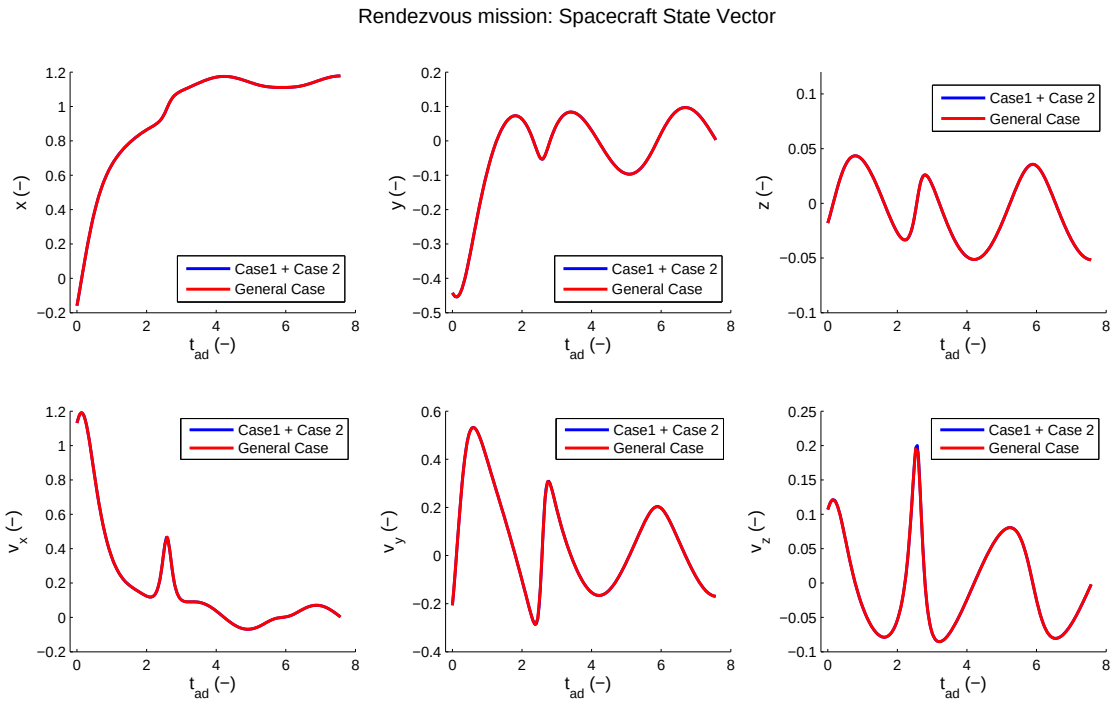

Figure A.1: Spacecraft state vector evolution during the rendezvous mission.

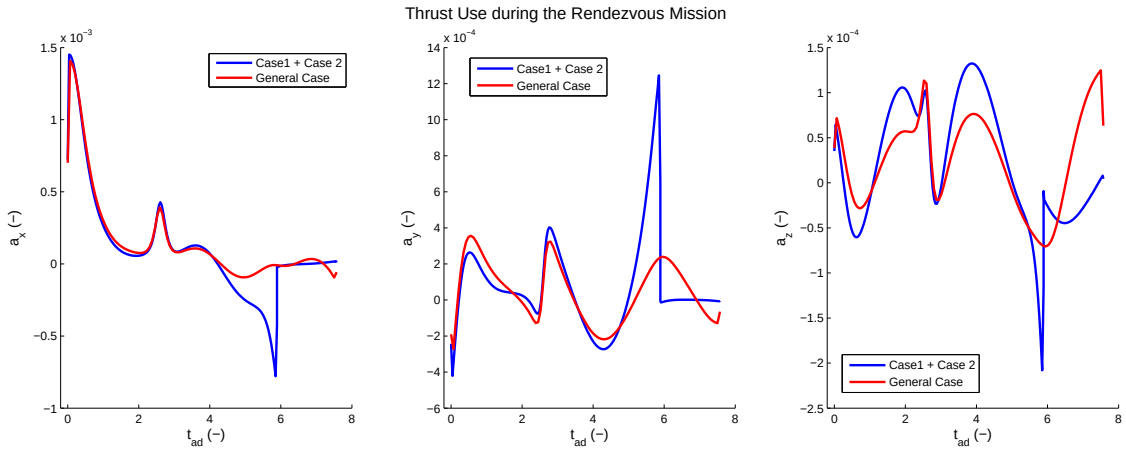

Figure A.2: Spacecraft state vector evolution during the rendezvous mission.